ESAIM: M2AN 57 (2023) 3007–3027
https://doi.org/10.1051/m2an/2023073

ESAIM: Mathematical Modelling and Numerical Analysis
www.esaim-m2an.org

A VIRTUAL ELEMENT METHOD FOR OVERCOMING LOCKING PHENOMENA IN BIOT'S CONSOLIDATION MODEL

Xin Liu[1] and Zhangxin Chen[2,*]

Abstract. A novel algorithm for the three-field formulation of Biot's consolidation model based on mixed and divergence-free nonconforming virtual element methods is developed and analyzed. By establishing a discrete counterpart of Korn's inequality, we ensure the well-posedness of this algorithm without special constraints in the context of nonconforming methods. In addition, we also derive a unified error estimate for this fully discrete algorithm no matter whether the specific storage coefficient vanishes or not. Moreover, this algorithm has several features, including supporting general polygonal meshes and arbitrary space approximation orders, and without Poisson's locking and pressure oscillations. Numerical experiments are presented to validate the performance of this algorithm.

Mathematics Subject Classification. 65N12, 65N15, 65N30, 74F10, 76S05.

Received October 31, 2022. Accepted August 31, 2023.

1. Introduction

Biot's consolidation model [1–3], as a description of the mechanical behavior of fluid-saturated porous media, is of great significance in a variety of science and engineering fields, including soil consolidation, geological carbon sequestration, petroleum production, perfusion of bones and soft living tissues [4–12]. In this paper, we restrict our study to the fully saturated incompressible poroelastic flow under small deformations; that is, the deformation of the porous media is governed by homogeneous and isotropic linear elasticity, whereas the motion of the fluid in the media is described by mass conservation and Darcy's law:

$$-\operatorname{div}\boldsymbol{\sigma} + \alpha\nabla p = \mathbf{f} \quad \text{in} \quad \Omega\times[0,T], \tag{1.1a}$$

$$\frac{\partial}{\partial t}(c_0 p + \alpha \operatorname{div}\mathbf{u}) + \operatorname{div}\mathbf{q} = g \quad \text{in} \quad \Omega\times[0,T], \tag{1.1b}$$

$$\kappa^{-1}\mathbf{q} + \nabla p = 0 \quad \text{in} \quad \Omega\times[0,T], \tag{1.1c}$$

with simple homogeneous boundary conditions and appropriate initial conditions:

$$\mathbf{u} = \mathbf{0} \quad \text{on } \Gamma_{uD}\times[0,T], \qquad (\boldsymbol{\sigma} - \alpha p\boldsymbol{I})\cdot\mathbf{n} = 0 \quad \text{on } \Gamma_{uN}\times[0,T], \tag{1.1d}$$

Keywords and phrases. Virtual element method, Biot's consolidation model, unified error estimate, Poisson locking and pressure oscillation, general polygonal meshes.

[1] School of Mathematics and Statistics, Northwestern Polytechnical University, Xi'an 710129, P.R. China.

[2] Department of Chemical and Petroleum Engineering, Schulich School of Engineering, University of Calgary, 2500 University Drive N.W., Calgary, Alberta T2N 1N4, Canada.

*Corresponding author: zhachen@ucalgary.ca

$$p = 0 \quad \text{on } \Gamma_{pD} \times [0,T], \qquad \mathbf{q}\cdot\mathbf{n} = 0 \quad \text{on } \Gamma_{pN} \times [0,T], \tag{1.1e}$$

$$\mathbf{u}(\cdot,0) = \mathbf{u}^0 \quad \text{in } \Omega, \qquad p(\cdot,0) = p^0 \quad \text{in } \Omega, \tag{1.1f}$$

where $\mathbf{u}$, $\mathbf{q}$ and p are the unknown displacement, fluid velocity and pressure, respectively, $\mathbf{f}$ is the body force on the solid, g is a fluid source/sink term, the Cauchy stress tensor is given by

$$\boldsymbol{\sigma} = 2\mu\,\varepsilon(\mathbf{u}) + \lambda(\operatorname{div}\mathbf{u})\boldsymbol{I}$$

with the Lamé constants λ and μ, the symmetric gradient operator $\varepsilon(\mathbf{u}) = (\nabla\mathbf{u} + \nabla^T\mathbf{u})/2$, and the identity matrix $\boldsymbol{I} \in \mathbb{R}^{2\times 2}$. $c_0 \geq 0$ and α are, respectively, the constrained specific storage coefficient and the Biot-Willis constant (close to one and related to the compressibility of the solid and fluid constituents), and κ is the permeability of a porous medium which is assumed isotropic and satisfies $0 < \kappa_1 \leq \kappa(\mathbf{x}) \leq \kappa_2 < \infty$ for all $\mathbf{x} \in \Omega$. Also, we consider Ω to be a bounded domain in $\mathbb{R}^2$ with boundary $\partial\Omega = \Gamma_{uD} \cup \Gamma_{uN} = \Gamma_{pD} \cup \Gamma_{pN}$ and the outward unit normal $\mathbf{n}$. In addition, we point out that the use of the three-field poroelastic model can avoid the postprocessing of the physically meaningful fluid velocity, and allow the application of physically meaningful boundary conditions at interfaces when considering the coupling between the fluid and poroelastic structures [13].

Then, the weak formulation of the three-field problem (1.1) can be introduced as follows: Find $(\mathbf{u}, \mathbf{q}, p) \in \mathbf{H}^1_{uD}(\Omega) \times \mathbf{H}_{pN}(\operatorname{div};\Omega) \times L^2(\Omega)$ for any time $t \in (0,T]$ such that

$$a(\mathbf{u},\mathbf{v}) - \alpha(p, \operatorname{div}\mathbf{v}) = (\mathbf{f},\mathbf{v}) \qquad \forall \mathbf{v} \in \mathbf{H}^1_{uD}(\Omega), \tag{1.2a}$$

$$c_0(p_t, w) + \alpha(\operatorname{div}\mathbf{u}_t, w) + (\operatorname{div}\mathbf{q}, w) = (g, w) \qquad \forall w \in L^2(\Omega), \tag{1.2b}$$

$$\tilde{a}(\mathbf{q},\mathbf{z}) - (p, \operatorname{div}\mathbf{z}) = 0 \qquad \forall \mathbf{z} \in \mathbf{H}_{pN}(\operatorname{div};\Omega), \tag{1.2c}$$

where the considered function spaces are

$$\mathbf{H}^1_{uD}(\Omega) := \big\{\mathbf{v} \in [H^1(\Omega)]^2 : \mathbf{v}|_{\Gamma_{uD}} = 0\big\},$$
$$\mathbf{H}_{pN}(\operatorname{div};\Omega) := \big\{\mathbf{z} \in \mathbf{H}(\operatorname{div};\Omega) : \mathbf{z}\cdot\mathbf{n}|_{\Gamma_{pN}} = 0\big\},$$

and the bilinear forms $a : \mathbf{H}^1_{uD}(\Omega) \times \mathbf{H}^1_{uD}(\Omega) \to \mathbb{R}$ and $\tilde{a} : \mathbf{H}_{pN}(\operatorname{div};\Omega) \times \mathbf{H}_{pN}(\operatorname{div};\Omega) \to \mathbb{R}$ are defined as

$$a(\mathbf{u},\mathbf{v}) = 2\mu(\varepsilon(\mathbf{u}),\varepsilon(\mathbf{v})) + \lambda(\operatorname{div}\mathbf{u}, \operatorname{div}\mathbf{v}), \qquad \tilde{a}(\mathbf{q},\mathbf{z}) = \big(\kappa^{-1}\mathbf{q},\mathbf{z}\big).$$

Results on the existence and uniqueness of a solution to the three-field Biot's consolidation model (1.2) were shown by Lipnikov in Theorem 2.1 of [14].

There is an extensive body of literature on numerical methods for Biot's consolidation model, *e.g.*, the finite difference [15–17], finite volume [18], and finite element [19–24] methods. However, as a common method, the standard Galerkin finite element method produces an oscillatory numerical behavior of pressure when the constrained specific storage coefficient is null (*i.e.*, $c_0 = 0$), the permeability κ of a porous medium is very low, and a large time step is used [25]. In general, this numerical instability can be attributed to the violation of an inf-sup condition [26] and the lack of the monotonicity of a discrete scheme [27]. At the same time, because the displacement in a linear poroelasticity problem tends to a divergence-free state as $\lambda \to \infty$ like in linear elasticity, continuous linear/bilinear finite elements on a triangular/rectangular mesh produce a poor approximation to the displacement, *i.e.*, Poisson-locking, as $\lambda \to \infty$ [26]. Therefore, to overcome these two modes of locking phenomena (*i.e.*, Poisson locking and pressure oscillation), some researchers combined a mixed finite element method for the flow variables and a nonconforming [28, 29]/discontinuous [30, 31]/weak [32] Galerkin method for displacement, possibly with some stabilization techniques [33–35]. Some other strategies can also be found in [36–40].

On the other hand, considering the complex geometric characteristics of practical poroelastic problems (especially with faults and heterogeneities) and the difficulty of the compatibility of an interface mesh when Biot's

model is coupled with other models, we are interested in developing numerical methods that allow more general meshes. The virtual element method (VEM) introduced in [41], as a new technique for the discretization of partial differential equations, not only avoids explicit expressions of basis functions (which helps to build high-order methods without complex integration), but also handles more general mesh partitions, including nonconvex, very distorted and curved-edge elements, and elements with hanging nodes. In addition, the study of its numerical implementation, including how to calculate the H^1- and L^2-projections and achieve the computability of discrete bilinear forms, can be found in [42]. Also, by combing the ideas of the VEM with other numerical methods, the H^α-conforming VEM [43], the nonconforming VEM [44], and $H(\mathrm{div})/H(\mathrm{curl})$-VEM [45,46] were proposed. Then, these VEMs have been applied to an increasing number of problems, such as two- and three-dimensional elasticity [47–49], incompressible fluids [50,51], plate bending [52,53], discrete fracture networks [54,55], and Cahn-Hillard problems [56,57].

In this work, we propose a novel space discretization method (standard choices are made for the time discretization) for problem (1.1) where the mixed [46] and divergence-free nonconforming [58] virtual element approximations for the pressure, fluid velocity and displacement are used, which is different from the mixed and conforming methods studied in [59]. Our method ensures the stability (expressed by a discrete counterpart of Korn's inequality) without adding a jump penalty term required for the nonconforming finite element method [28,29], when designing the linear elasticity operator. Moreover, this method is shown to be free of both Poisson locking as $\lambda \to \infty$ and pressure oscillation in the case of $c_0 = 0$, a low permeability, and a large time step size. Furthermore, it inherits the features of the VEM, which allows to use general polygonal meshes (including meshes with hanging nodes) and to increase the space approximation in order to accelerate convergence. Finally, we also obtain a unified optimal error estimate for this fully discrete method when $c_0 > 0$ and $c_0 = 0$.

The rest of this paper is organized as follows: In Section 2, we introduce some discrete settings and formulate the proposed method. In Section 3, we carry out the stability and convergence analyses for this method. In Section 4, numerical tests are presented to validate the theory. Finally, we conclude in Section 5.

2. Construction of the discrete scheme

In this section, we first give some preliminaries, then introduce the definitions of the divergence-free nonconforming and mixed virtual element two-dimensional spaces, and finally design the discrete counterparts of the elasticity and Darcy operators to form a fully discrete virtual element scheme.

2.1. Preliminaries

Let $\mathcal{T}_h$ be a decomposition of Ω into polygonal elements K with the maximum element size $h = \max_{K\in\mathcal{T}_h} \mathrm{diam}(K)$. All edges in $\mathcal{T}_h$ are collected in the set $\mathcal{E}_h = \mathcal{E}_h^i \cup \mathcal{E}_h^b$ with $\mathcal{E}_h^i$ and $\mathcal{E}_h^b$ being the sets of interior and boundary edges in mesh $\mathcal{T}_h$. $N_\mathcal{T}$ and $N_\mathcal{E}$ are introduced as the total numbers of elements and edges in $\mathcal{T}_h$. The mesh partition $\mathcal{T}_h$ is assumed to be shape-regular in the following sense:

Assumption (A0) ([41, 44])**.** We assume that for every h, decomposition $\mathcal{T}_h$ is made of a finite number of simple polygons. There exists a positive real number γ such that the following properties hold: (i) for every element K, the distance between any two vertices in K is $\geq \gamma\mathrm{diam}(K)$; (ii) every element K is star-shaped with respect to a ball of radius $\geq \gamma\mathrm{diam}(K)$.

For later use, we use notation $\mathbf{n}_e$ for the unit normal vector of edge $e \in \mathcal{E}_h$ with a fixed orientation and the corresponding anticlockwise tangential vector can be defined as $\mathbf{t}_e$, while $\mathbf{n}_K/\mathbf{t}_K$ can be defined as the exterior unit normal/anticlockwise tangential vector of element K. Also, for an interface e shared by $K^+, K^- \in \mathcal{T}_h$ with the unit normal vector $\mathbf{n}_e$ pointing from K^+ to K^-, if $\cdot|_{K_e^\pm}$ represents the trace of a function on e taken from the element $K^\pm$, we can define the jump operator of a scalar/vector function w by $[\![w]\!] := w|_{K_e^+} - w|_{K_e^-}$; similarly, for a boundary edge e shared by $\partial\Omega$ and $K^+ \in \mathcal{T}_h$, we have $[\![w]\!] := w|_{K_e^+}$. Moreover, we also consider a uniform partition of the time interval $[0, T]$, *i.e.*, the time step is $\tau = T/N$ with the time layer $N \in \mathbb{N}^*$, and set $\chi^n := \chi(t^n)$ with a discrete time $t^n = n\tau$ for all $0 \leq n \leq N$.

In what follows, we use the standard notation for the Sobolev spaces and trace, div, rot, **curl** operators, and define the set of polynomials of degree less than or equal to ℓ on a domain $\mathcal{D}$ by $\mathbb{P}_\ell(\mathcal{D})$; especially, $\mathbb{P}_{-1}(\mathcal{D}) = \{0\}$. Then, we introduce some useful operators:

– The local H^1-projection $\Pi_k^{\nabla,K} : [H^1(K)]^2 \to [\mathbb{P}_k(K)]^2$ on K is defined by

$$\begin{cases} \displaystyle\int_K \nabla\left(\Pi_k^{\nabla,K}\mathbf{v} - \mathbf{v}\right) : \nabla\mathbf{m}\,\mathrm{d}x = 0 & \forall \mathbf{m} \in [\mathbb{P}_k(K)]^2, \\ \displaystyle\int_{\partial K}\left(\Pi_k^{\nabla,K}\mathbf{v} - \mathbf{v}\right)\mathrm{d}x = 0 & \forall \mathbf{v} \in [H^1(K)]^2; \end{cases} \tag{2.1}$$

– The local L^2-projection $\Pi_k^{0,K} : [L^2(K)]^2 \to [\mathbb{P}_k(K)]^2$ on K is defined by

$$\left(\Pi_k^{0,K}\mathbf{v}, \mathbf{m}\right)_K = (\mathbf{v}, \mathbf{m})_K \qquad \forall \mathbf{m} \in [\mathbb{P}_k(K)]^2; \tag{2.2}$$

– The composite operators $\Pi_{k-1}^{0,K} \circ \varepsilon$ and $\Pi_{k-1}^{0,K} \circ \mathrm{div}$ are defined by

$$\begin{aligned} \left(\Pi_{k-1}^{0,K}\varepsilon(\mathbf{v}), \mathbf{m}\right)_K &= (\varepsilon(\mathbf{v}), \mathbf{m})_K \qquad \forall \mathbf{m} \in [\mathbb{P}_{k-1}(K)]^{2\times 2}, \\ \left(\Pi_{k-1}^{0,K}\mathrm{div}\,\mathbf{v}, m\right)_K &= (\mathrm{div}\,\mathbf{v}, m)_K \qquad \forall m \in \mathbb{P}_{k-1}(K). \end{aligned} \tag{2.3}$$

Additionally, the H^1- and L^2-projections satisfy the following approximation properties [41, 60]: For every $\mathbf{v} \in [H^{s+1}(K)]^2$, there exists a positive constant C, depending on the polynomial degree k and the mesh regularity constant γ, such that

$$\begin{aligned} \left\|\mathbf{v} - \Pi_k^{\nabla,K}\mathbf{v}\right\|_{m,K} &\le Ch_K^{s+1-m}|\mathbf{v}|_{s+1,K} \qquad m \in \mathbb{N}, \max(m-1,0) \le s \le k, \\ \left\|\mathbf{v} - \Pi_k^{0,K}\mathbf{v}\right\|_{m,K} &\le Ch_K^{s+1-m}|\mathbf{v}|_{s+1,K} \qquad m \in \mathbb{N}, m-1 \le s \le k. \end{aligned} \tag{2.4}$$

Remark 2.1. The computability of these operators needs to be discussed based on the specific virtual element discrete spaces, which can be found in Section 2.2.

2.2. Definitions of virtual element discrete spaces

We introduce the Raviart–Thomas-like virtual element space for the fluid velocity [45]:

$$\begin{aligned} \mathbf{Z}_h = \{\mathbf{z}_h \in \mathbf{H}_{pN}(\mathrm{div};\Omega) : {} & (\mathbf{z}_h \cdot \mathbf{n}_e)|_e \in \mathbb{P}_{k-1}(e) && \forall e \in \mathcal{E}_h, \\ & (\mathrm{div}\,\mathbf{z}_h)|_K \in \mathbb{P}_{k-1}(K), \quad (\mathrm{rot}\,\mathbf{z}_h)|_K \in \mathbb{P}_{k-2}(K) && \forall K \in \mathcal{T}_h\}, \end{aligned}$$

and the piecewise polynomial function space for the pressure:

$$W_h = \left\{w_h \in L^2(\Omega) : w_h|_K \in \mathbb{P}_{k-1}(K) \quad \forall K \in \mathcal{T}_h\right\}.$$

Obviously, the dimension of $\mathbf{Z}_h$ is given by $kN_\mathcal{E} + (\frac{(k+1)k}{2} - 1 + \frac{k(k-1)}{2})N_\mathcal{T}$ and its corresponding unisolvent degrees of freedom are the following three types [45]:

d1. The moment $\frac{1}{|e|}\int_e \mathbf{z}_h \cdot \mathbf{n}_e m\,\mathrm{d}s$ for $m \in \mathbb{P}_{k-1}(e)$ on each edge $e \in \mathcal{E}_h$, where $|e|$ represents the measure of edge e;

d2. The moment $\frac{1}{|K|}\int_K \mathbf{z}_h \cdot \nabla m\,\mathrm{d}x$ for $m \in \mathbb{P}_{k-1}(K)/\mathbb{R}$ in each element $K \in \mathcal{T}_h$, where $|K|$ represents the area of polygon K;

d3. The moment $\frac{1}{|K|}\int_K \mathbf{z}_h \cdot \mathbf{g}_{k-1}^\perp\,\mathrm{d}x$ for $\mathbf{g}_{k-1}^\perp \in \mathcal{G}_{k-1}^\perp(K) := \begin{bmatrix} y \\ -x \end{bmatrix}\mathbb{P}_{k-2}(K)$ in each element $K \in \mathcal{T}_h$.

Let $w_I \in W_h$ and $\mathbf{z}_I \in \mathbf{Z}_h$ be the virtual element interpolants, *i.e.*, for a given $w \in L^2(\Omega)$ and $\mathbf{z} \in \mathbf{H}_{pN}(\mathrm{div};\Omega) \cap [L^s(\Omega)]^2$ (for some $s > 2$), they, respectively, hold

$$\int_K (w - w_I) m \,\mathrm{d}x = 0 \qquad \forall K \in \mathcal{T}_h,\ \forall m \in \mathbb{P}_{k-1}(K)$$

and

$$\varrho_i^{\mathbf{Z}}(\mathbf{z} - \mathbf{z}_I) = 0 \qquad i = 1, 2, \ldots, \dim \mathbf{Z}_h,$$

where operator $\varrho_i^{\mathbf{Z}}$ is associated to the i-th degree of freedom of $\mathbf{Z}_h$. Additionally, it has been shown in (4.3) of [46] and Theorem 3.4 of [61] that, for every $\mathbf{z} \in [H^{\ell+1}(K)]^2$, $\mathrm{div}\,\mathbf{z} \in H^\ell(K)$ and $w \in H^\ell(K)$ with $0 \le \ell \le k$, we have

$$\begin{aligned} w_I &= \Pi_{k-1}^{0,K} w, & \mathrm{div}\,\mathbf{z}_I &= \Pi_{k-1}^{0,K} \mathrm{div}\,\mathbf{z}, \\ \|w - w_I\|_{0,K} &\le C h_K^\ell \|w\|_{\ell,K}, & \|\mathrm{div}\,\mathbf{z} - \mathrm{div}\,\mathbf{z}_I\|_{0,K} &\le C h_K^\ell \|\mathrm{div}\,\mathbf{z}\|_{\ell,K}, \end{aligned} \tag{2.5}$$

and when $\mathbf{z}_\pi \in [\mathbb{P}_k(K)]^2$ is an optimal local polynomial approximation, we obtain

$$\|\mathbf{z} - \mathbf{z}_I\|_{0,K} + \|\mathbf{z} - \mathbf{z}_\pi\|_{0,K} \le C h_K^{\ell+1} \|\mathbf{z}\|_{\ell+1,K}, \tag{2.6}$$

where constant C depends only on the polynomial degree k and the mesh regularity constant γ. Furthermore, referring to Corollary 5.5 in [46], it follows that there exists a constant $\tilde{\beta} > 0$, independent of the mesh size h, such that

$$\sup_{\mathbf{z}_h \in \mathbf{Z}_h \setminus \{0\}} \frac{(\mathrm{div}\,\mathbf{z}_h, w_h)}{\|\mathbf{z}_h\|_{\mathbf{H}(\mathrm{div})}} \ge \tilde{\beta} \|w_h\|_0 \qquad \forall w_h \in W_h. \tag{2.7}$$

Remark 2.2. To ensure the computability of operator $\Pi_{k-1}^{0,K}$ defined in the local space $\mathbf{Z}_h|_K$, we need to realize $(\mathbf{z}_h, \mathbf{m})_K$ for $\mathbf{m} \in [\mathbb{P}_{k-1}(K)]^2$ only by the degrees of freedom of $\mathbf{Z}_h|_K$, *i.e.*,

$$(\mathbf{z}_h, \mathbf{m})_K = (\mathbf{z}_h, \nabla p_k)_K + \left(\mathbf{z}_h, \mathbf{g}_{k-1}^\perp\right)_K = -(\mathrm{div}\,\mathbf{z}_h, p_k)_K + \langle \mathbf{z}_h \cdot \mathbf{n}, p_k \rangle_{\partial K} + \left(\mathbf{z}_h, \mathbf{g}_{k-1}^\perp\right)_K,$$

where, in the first equality, we use the fact that every polynomial $\mathbf{m} \in [\mathbb{P}_{k-1}(K)]^2$ can be uniquely divided into $\nabla p_k \in \nabla \mathbb{P}_k(K)$ and $\mathbf{g}_{k-1}^\perp \in \mathcal{G}_{k-1}^\perp(K)$. For more details, the reader can refer to [42].

Next, for any element $K \in \mathcal{T}_h$, the local discrete space for the displacement can be defined as [58]

$$\mathbf{X}_{h|K} = \boldsymbol{\Theta}(K) + \mathbf{curl} S(K),$$

where $\boldsymbol{\Theta}(K)$ is the local Brezzi–Douglas–Marini-like virtual element space defined by

$$\boldsymbol{\Theta}(K) = \left\{ \boldsymbol{\theta}_h \in [H^1(K)]^2 : \boldsymbol{\theta}_h \cdot \mathbf{n}_e|_e \in \mathbb{P}_k(e) \ \ \forall e \in \partial K, \ \ \mathrm{div}\,\boldsymbol{\theta}_h \in \mathbb{P}_{k-1}(K), \ \ \mathrm{rot}\,\boldsymbol{\theta}_h \in \mathbb{P}_{k-1}(K) \right\}$$

and $S(K)$ is the local H^2-virtual element space defined by

$$S(K) = \left\{ \psi_h \in H^2(K) : \Delta^2 \psi_h \in \mathbb{P}_{k-3}(K), \quad \psi_h|_e = 0, \ \Delta \psi_h|_e \in \mathbb{P}_{k-1}(e) \ \ \forall e \in \partial K \right\}.$$

Then, for $\mathbf{H}_{uD}(\mathrm{div};\Omega) = \{\mathbf{v} \in \mathbf{H}(\mathrm{div};\Omega) : \mathbf{v} \cdot \mathbf{n}|_{\Gamma_{uD}} = \mathbf{0}\}$, the global discrete space $\mathbf{X}_h$ is introduced as

$$\begin{aligned} \mathbf{X}_h = \Big\{ & \mathbf{v}_h \in \mathbf{H}_{uD}(\mathrm{div};\Omega) : \mathbf{v}_h|_K \in \mathbf{X}_{h|K} \quad \forall K \in \mathcal{T}_h, \\ & \int_e [\![\mathbf{v}_h \cdot \mathbf{t}_e]\!] \cdot m \,\mathrm{d}s = 0 \quad \forall m \in \mathbb{P}_{k-1}(e), e \in \mathcal{E}_h \Big\}, \end{aligned}$$

equipped with the norm

$$|\mathbf{v}_h|_{1,h} := \left(\sum_{K \in \mathcal{T}_h} \|\nabla \mathbf{v}_h\|_{0,K}^2 \right)^{1/2}.$$

Referring to [62], it is not difficult to see that the unisolvent degrees of freedom for $\mathbf{X}_h$ can be divided into the following four types:

D1. The moment $\frac{1}{|e|}\int_e \mathbf{v}_h \cdot \mathbf{n}_e m \,\mathrm{d}s$ for $m \in \mathbb{P}_k(e)$ on each edge $e \in \mathcal{E}_h$;
D2. The moment $\frac{1}{|e|}\int_e \mathbf{v}_h \cdot \mathbf{t}_e m \,\mathrm{d}s$ for $m \in \mathbb{P}_{k-1}(e)$ on each edge $e \in \mathcal{E}_h$;
D3. The moment $\frac{1}{|K|}\int_K \operatorname{div} \mathbf{v}_h m \,\mathrm{d}s$ for $m \in \mathbb{P}_{k-1}(K)/\mathbb{R}$ in each element $K \in \mathcal{T}_h$;
D4. The moment $\frac{1}{|K|}\int_K \mathbf{v}_h \cdot \mathbf{g}_{k-2}^{\perp} \,\mathrm{d}s$ for $\mathbf{g}_{k-2}^{\perp} \in \mathcal{G}_{k-2}^{\perp}(K) := \begin{bmatrix} y \\ -x \end{bmatrix} \mathbb{P}_{k-3}(K)$ in each element $K \in \mathcal{T}_h$.

It is observed from (3.22) in [62] that $\operatorname{div}_h \mathbf{X}_h \subseteq W_h$ with div_h being the discrete version of the divergence operator div (*i.e.*, $\operatorname{div}_h|_K = \operatorname{div}$ for every $K \in \mathcal{T}_h$), which implies

$$\operatorname{div} \mathbf{v}_I = \Pi_{k-1}^{0,K} \operatorname{div} \mathbf{v} \qquad \forall \mathbf{v} \in \mathbf{H}_{uD}^1(\Omega), \tag{2.8}$$

where the virtual element interpolant $\mathbf{v}_I \in \mathbf{X}_h$ satisfies

$$\varrho_i^{\mathbf{X}}(\mathbf{v} - \mathbf{v}_I) = 0 \qquad i = 1, 2, \ldots, \dim \mathbf{X}_h$$

for operator $\varrho_i^{\mathbf{X}}$ associated to the i-th degree of freedom of $\mathbf{X}_h$. Then, referring to Lemmas 3.4 and 3.5 in [62], there exist $\mathbf{v}_I \in \mathbf{X}_{h|K}$ and $\mathbf{v}_\pi \in [\mathbb{P}_k(K)]^2$ such that for every $\mathbf{v} \in [H^{s+1}(K)]^2$ with $0 \le s \le k$

$$\begin{aligned} \|\mathbf{v} - \mathbf{v}_\pi\|_{0,K} + h_K \|\mathbf{v} - \mathbf{v}_\pi\|_{1,K} &\le C h_K^{s+1} \|\mathbf{v}\|_{s+1,K}, \\ \|\mathbf{v} - \mathbf{v}_I\|_{0,K} + h_K |\mathbf{v} - \mathbf{v}_I|_{1,K} &\le C h_K^{s+1} \|\mathbf{v}\|_{s+1,K}, \end{aligned} \tag{2.9}$$

where C is a positive constant depending only on the polynomial degree k and the mesh regularity constant γ. Moreover, we also introduce the inf-sup condition from (5.7) in [58]: There exists a constant $\beta > 0$, independent of the mesh size h, such that

$$\sup_{\mathbf{v}_h \in \mathbf{X}_h \setminus \{0\}} \frac{(\operatorname{div} \mathbf{v}_h, w_h)}{|\mathbf{v}_h|_{1,h}} \ge \beta \|w_h\|_0 \qquad \forall w_h \in W_h. \tag{2.10}$$

Remark 2.3. When these four operators (2.1)–(2.3) are defined on the local virtual element discrete space $\mathbf{X}_{h|K}$, their computability is similar. Taking $\Pi_k^{\nabla,K}$ as an example, the key to the realization of its computability is how to calculate $(\nabla \mathbf{v}_h, \nabla \mathbf{m})_K$ for $\mathbf{m} \in [\mathbb{P}_k(K)]^2$ through the degrees of freedom of the local space $\mathbf{X}_{h|K}$, *i.e.*,

$$\begin{aligned} (\nabla \mathbf{v}_h, \nabla \mathbf{m})_K &= -(\mathbf{v}_h, \Delta \mathbf{m})_K + (\mathbf{v}_h, \nabla \mathbf{m} \cdot \mathbf{n}_K)_{\partial K} \\ &= -\left(\mathbf{v}_h, \nabla p_{k-1} + \mathbf{g}_{k-2}^{\perp}\right)_K + \left(\mathbf{v}_h \cdot \mathbf{n}_K, (\nabla \mathbf{m})^T : (\mathbf{n}_K \otimes \mathbf{n}_K)\right)_{\partial K} \\ &\quad + \left(\mathbf{v}_h \cdot \mathbf{t}_K, (\nabla \mathbf{m})^T : (\mathbf{n}_K \otimes \mathbf{t}_K)\right)_{\partial K} \\ &= (\operatorname{div} \mathbf{v}_h, p_{k-1})_K - \left(\mathbf{v}_h, \mathbf{g}_{k-2}^{\perp}\right)_K + \left(\mathbf{v}_h \cdot \mathbf{n}_K, (\nabla \mathbf{m})^T : (\mathbf{n}_K \otimes \mathbf{n}_K) - p_{k-1}\right)_{\partial K} \\ &\quad + \left(\mathbf{v}_h \cdot \mathbf{t}_K, (\nabla \mathbf{m})^T : (\mathbf{n}_K \otimes \mathbf{t}_K)\right)_{\partial K}, \end{aligned}$$

where, in the second equality, we use the equivalent deformation of the boundary term $(\mathbf{v}_h, \nabla \mathbf{m} \cdot \mathbf{n}_K)_{\partial K}$ and the fact that $\Delta \mathbf{m} \in [\mathbb{P}_{k-2}(K)]^2$ can be uniquely decomposed into $\nabla p_{k-1} + \mathbf{g}_{k-2}^{\perp}$ for $p_{k-1} \in \mathbb{P}_{k-1}(K)$ and $\mathbf{g}_{k-2}^{\perp} \in \mathcal{G}_{k-2}^{\perp}(K)$.

2.3. Construction of the virtual element discrete method

Firstly, the local discrete approximations of the Darcy and linear elasticity operators can be designed as $\tilde{a}_h^K$ on $\mathbf{Z}_h|_K \times \mathbf{Z}_h|_K$ and a_h^K on $\mathbf{X}_{h|K} \times \mathbf{X}_{h|K}$, *i.e.*, for every $\mathbf{q}_h, \mathbf{z}_h \in \mathbf{Z}_h|_K$ and $\mathbf{u}_h, \mathbf{v}_h \in \mathbf{X}_{h|K}$,

$$\tilde{a}_h^K(\mathbf{q}_h, \mathbf{z}_h) = \left(\kappa^{-1}\left(\Pi_{k-1}^{0,K}\mathbf{q}_h\right), \Pi_{k-1}^{0,K}\mathbf{z}_h\right)_K + \tilde{S}^K\left(\mathbf{q}_h - \Pi_{k-1}^{0,K}\mathbf{q}_h, \mathbf{z}_h - \Pi_{k-1}^{0,K}\mathbf{z}_h\right), \tag{2.11a}$$

$$a_h^K(\mathbf{u}_h, \mathbf{v}_h) = 2\mu\left[\left(\Pi_{k-1}^{0,K}\varepsilon(\mathbf{u}_h), \Pi_{k-1}^{0,K}\varepsilon(\mathbf{v}_h)\right)_K + S^K\left(\mathbf{u}_h - \Pi_k^{\nabla,K}\mathbf{u}_h, \mathbf{v}_h - \Pi_k^{\nabla,K}\mathbf{v}_h\right)\right]$$

$$+\lambda\Big(\Pi_{k-1}^{0,K}\operatorname{div}\mathbf{u}_h,\Pi_{k-1}^{0,K}\operatorname{div}\mathbf{v}_h\Big)_K, \tag{2.11b}$$

with the stabilization bilinear forms $\tilde{S}^K$ [61] and S^K [58] satisfying

$$\begin{aligned}
&\tilde{c}_*\big(\kappa^{-1}\mathbf{z}_h,\mathbf{z}_h\big)_K\le\tilde{S}^K(\mathbf{z}_h,\mathbf{z}_h)\le\tilde{c}^*(\kappa^{-1}\mathbf{z}_h,\mathbf{z}_h)_K &&\forall\mathbf{z}_h\in\ker\Big(\Pi_{k-1}^{0,K}\Big),\\
&c_*(\nabla\mathbf{v}_h,\nabla\mathbf{v}_h)_K\le S^K(\mathbf{v}_h,\mathbf{v}_h)\le c^*(\nabla\mathbf{v}_h,\nabla\mathbf{v}_h)_K &&\forall\mathbf{v}_h\in\ker\Big(\Pi_k^{\nabla,K}\Big),
\end{aligned}\tag{2.12}$$

for some positive constants $\tilde{c}_*,\tilde{c}^*$ and c_*,c^* independent of h.

Remark 2.4. If we want to use operator $\Pi_k^{0,K}$ instead of $\Pi_{k-1}^{0,K}$ in our discrete scheme (2.11a), we need to introduce the corresponding Brezzi–Douglas–Marini-like virtual element space instead of the Raviart–Thomas-like virtual element space.

Remark 2.5. In the construction of the stabilization bilinear form in (2.11b), we used $S^K(\mathbf{u}_h-\Pi_k^{\nabla,K}\mathbf{u}_h,\mathbf{v}_h-\Pi_k^{\nabla,K}\mathbf{v}_h)$, which corresponds to the stabilization of the H^1 inner product rather than that of the symmetric gradient inner product, but this does not affect the subsequent theoretical results. And it is worth mentioning that the stability bounds of S^K in (2.12) are obtained from a simple scaling argument, and there is currently no rigorous stability results for the space $\mathbf{X}_h$, which is beyond the scope of this paper and may be studied in our future work.

It is evident that the bilinear forms $\tilde{a}_h^K(\cdot,\cdot)$ and $a_h^K(\cdot,\cdot)$ satisfy the k-consistency:

$$\begin{aligned}
&\tilde{a}_h^K(\mathbf{m},\mathbf{z}_h)=\Big(\kappa^{-1}\mathbf{m},\Pi_{k-1}^{0,K}\mathbf{z}_h\Big)_K && \text{for every } \mathbf{z}_h\in\mathbf{Z}_h|_K,\mathbf{m}\in[\mathbb{P}_{k-1}(K)]^2,\\
&a_h^K(\mathbf{m},\mathbf{v}_h)=2\mu\Big(\varepsilon(\mathbf{m}),\Pi_{k-1}^{0,K}\varepsilon(\mathbf{v}_h)\Big)_K+\lambda(\operatorname{div}\mathbf{m},\operatorname{div}\mathbf{v}_h)_K && \text{for every } \mathbf{v}_h\in\mathbf{X}_{h|K},\mathbf{m}\in[\mathbb{P}_k(K)]^2,
\end{aligned}\tag{2.13}$$

and the continuity and coercivity:

$$\begin{aligned}
&\tilde{a}_h^K(\mathbf{q}_h,\mathbf{z}_h)\le\tilde{C}^*\Big\|\kappa^{-\frac{1}{2}}\mathbf{q}_h\Big\|_{0,K}\Big\|\kappa^{-\frac{1}{2}}\mathbf{z}_h\Big\|_{0,K} &&\forall\mathbf{q}_h,\mathbf{z}_h\in\mathbf{Z}_h|_K,\\
&\tilde{a}_h^K(\mathbf{z}_h,\mathbf{z}_h)\ge\tilde{C}_*\Big\|\kappa^{-\frac{1}{2}}\mathbf{z}_h\Big\|_{0,K}^2 &&\forall\mathbf{z}_h\in\mathbf{Z}_h|_K,\\
&a_h^K(\mathbf{u}_h,\mathbf{v}_h)\le C^*\|\nabla\mathbf{u}_h\|_{0,K}\|\nabla\mathbf{v}_h\|_{0,K} &&\forall\mathbf{u}_h,\mathbf{v}_h\in\mathbf{X}_{h|K}.
\end{aligned}\tag{2.14}$$

Additionally, we can prove the following discrete Korn's inequality, which helps to derive the coercivity of the bilinear form $a_h^K(\cdot,\cdot)$:

Lemma 2.6. *There exists a positive constant C, depending only on the mesh regularity constant γ, such that, for every $\mathbf{v}_h\in\mathbf{X}_h$ and the element-wise symmetric gradient $\varepsilon_h(\mathbf{v}_h)$,*

$$|\mathbf{v}_h|_{1,h}\le C\|\varepsilon_h(\mathbf{v}_h)\|_0.$$

Proof. Imitating a broken Korn's inequality in Theorem 3.1 in [63], we can obtain

$$|\mathbf{v}_h|_{1,h}^2\le C\left(\|\varepsilon_h(\mathbf{v}_h)\|_0^2+\sum_{e\in\mathcal{E}_h^i}(\operatorname{diam}\ e)^{-1}\|\Pi_e[\![\mathbf{v}_h]\!]\|_{0,e}^2+\left|\sum_{K\in\mathcal{T}_h}\int_K\operatorname{rot}\mathbf{v}_h\,\mathrm{d}x\right|^2\right),\tag{2.15}$$

where $\mathcal{E}_h^i$ represents the set of interelement edges of the mesh and Π_e is the L^2-projection to $\mathcal{P}_1(e)=\{\mathbf{m}\in[\mathbb{P}_1(e)]^2:$ the tangential component of $\mathbf{m}$ belongs to $\mathbf{RM}(e)\}$ with $\mathbf{RM}(e)$ being the space of rigid motions on edge e.

Due to the continuity of the normal component of $\mathbf{v}_h$ with respect to linear polynomials and the continuity of the tangential component of $\mathbf{v}_h$ with respect to constants on the internal edges, it holds that $\int_e [\![\mathbf{v}_h]\!]\cdot\mathbf{m}\,\mathrm{d}s = 0$ for any $e \in \mathcal{E}_h^i$ and $\mathbf{m} \in \mathcal{P}_1(e)$. From the definition of the L^2-projection Π_e, we have $\|\Pi_e[\![\mathbf{v}_h]\!]\|_{0,e}^2 = 0$ for any $e \in \mathcal{E}_h^i$. Also, the last term in the above formula vanishes from the integration by part and the fact $\int_e [\![\mathbf{v}_h \cdot \mathbf{t}_e]\!]\,\mathrm{d}s = 0$ for any $e \in \mathcal{E}_h$. Thus, the desired result will be obtained. □

Remark 2.7. The proof of (2.15) can be divided into three steps: firstly, introducing a well-defined interpolation operator and giving its approximation properties according to Corollary A.3 and (3.4) in [64]; secondly, proving the generalized Korn's inequality for piecewise linear vector fields following Lemma 2.2 in [64]; finally, using the triangular inequality, and combining the above results with the inverse (*cf.* [58], Lem. 24) and trace (*cf.* [62], (5.19)) inequalities to show the conclusion. For more details, please refer to Theorem 3.1 in [63].

Secondly, we realize the discretizations of the coupling terms $-\alpha(p, \operatorname{div}\mathbf{v}), (\operatorname{div}\mathbf{q}, w)$ and the right-hand term $(\mathbf{f}, \mathbf{v})$ by proposing the local bilinear forms b_h^K on $\mathbf{X}_{h|K} \times W_h|_K$, c_h^K on $\mathbf{Z}_h|_K \times W_h|_K$, and the discrete duality product $\langle\cdot,\cdot\rangle_h$, *i.e.*, for every $\mathbf{v}_h \in \mathbf{X}_{h|K}$, $p_h, w_h \in W_h|_K$ and $\mathbf{q}_h \in \mathbf{Z}_h|_K$,

$$b_h^K(\mathbf{v}_h, p_h) = -\alpha\Big(p_h, \Pi_{k-1}^{0,K}\operatorname{div}\mathbf{v}_h\Big)_K = -\alpha(p_h, \operatorname{div}\mathbf{v}_h)_K, \tag{2.16a}$$

$$c_h^K(\mathbf{q}_h, w_h) = \Big(\Pi_{k-1}^{0,K}\operatorname{div}\mathbf{q}_h, w_h\Big)_K = (\operatorname{div}\mathbf{q}_h, w_h)_K, \tag{2.16b}$$

$$\langle \mathbf{f}_h, \mathbf{v}_h\rangle_h = \sum_{K\in\mathcal{T}_h}\int_K \mathbf{f}\cdot\Pi_k^{0,K}\mathbf{v}_h\,\mathrm{d}x \quad \text{with} \quad \mathbf{f}_{h|K} = \Pi_k^{0,K}\mathbf{f}. \tag{2.16c}$$

Also, it is easy to obtain the local discrete forms of term $\alpha(\operatorname{div}\mathbf{u}_t, w)$ by $\alpha(\Pi_{k-1}^{0,K}\operatorname{div}\mathbf{u}_{ht}, w_h)_K$ and term $-(p, \operatorname{div}\mathbf{z})$ by $-(p_h, \Pi_{k-1}^{0,K}\operatorname{div}\mathbf{z}_h)_K$, which can be expressed as $-b_h^K(\mathbf{u}_{ht}, w_h)$ and $-c_h^K(\mathbf{z}_h, p_h)$, respectively.

Finally, we can obtain the global discrete forms $\tilde{a}_h(\cdot,\cdot), a_h(\cdot,\cdot), b_h(\cdot,\cdot)$, and $c_h(\cdot,\cdot)$ by simply summing their respective local contributions and give the fully discrete virtual element method for Biot's problem at each time t^n $(1 \le n \le N)$: Find $(\mathbf{u}_h^n, \mathbf{q}_h^n, p_h^n) \in \mathbf{X}_h \times \mathbf{Z}_h \times W_h$ such that

$$a_h(\mathbf{u}_h^n, \mathbf{v}_h) + b_h(\mathbf{v}_h, p_h^n) = \langle \mathbf{f}_h^n, \mathbf{v}_h\rangle_h \qquad \forall \mathbf{v}_h \in \mathbf{X}_h, \tag{2.17a}$$

$$c_0(\partial_t p_h^n, w_h) - b_h(\partial_t \mathbf{u}_h^n, w_h) + c_h(\mathbf{q}_h^n, w_h) = (g^n, w_h) \qquad \forall w_h \in W_h, \tag{2.17b}$$

$$\tilde{a}_h(\mathbf{q}_h^n, \mathbf{z}_h) - c_h(\mathbf{z}_h, p_h^n) = 0 \qquad \forall \mathbf{z}_h \in \mathbf{Z}_h, \tag{2.17c}$$

with the given initial values $(\mathbf{u}_I^0, p_I^0)$ (*i.e.*, the values of the virtual element interpolations $(\mathbf{u}_I, p_I)$ at time t^0), where operator ∂_t can be defined as the backward Euler difference:

$$\partial_t \chi^n = \frac{\chi^n - \chi^{n-1}}{\tau}.$$

3. Numerical analysis for the fully discrete method

In this section, we discuss the existence and uniqueness of a solution for the fully discrete method at each time step t^n and investigate its unified error estimate with $c_0 \ge 0$.

3.1. Well-posedness

Let us rewrite equation (2.17) as the following saddle point problem:

$$\mathcal{A}_h((\mathbf{u}_h^n, \mathbf{q}_h^n), (\mathbf{v}_h, \mathbf{z}_h)) + \mathcal{B}_h((\mathbf{v}_h, \mathbf{z}_h), p_h^n) = \langle \mathbf{f}_h^n, \mathbf{v}_h\rangle_h \qquad \forall (\mathbf{v}_h, \mathbf{z}_h) \in \mathbf{X}_h \times \mathbf{Z}_h, \tag{3.1a}$$

$$\mathcal{B}_h((\mathbf{u}_h^n, \mathbf{q}_h^n), w_h) - \mathcal{C}_h(p_h^n, w_h) = -\tau(g^n, w_h) + b_h\big(\mathbf{u}_h^{n-1}, w_h\big) - c_0\big(p_h^{n-1}, w_h\big) \qquad \forall w_h \in W_h, \tag{3.1b}$$

where the bilinear forms are defined by

$$\begin{aligned}\mathcal{A}_h((\mathbf{u}_h,\mathbf{q}_h),(\mathbf{v}_h,\mathbf{z}_h)) &= a_h(\mathbf{u}_h,\mathbf{v}_h)+\tau\tilde{a}_h(\mathbf{q}_h,\mathbf{z}_h),\\ \mathcal{B}_h((\mathbf{v}_h,\mathbf{z}_h),p_h) &= b_h(\mathbf{v}_h,p_h)-\tau c_h(\mathbf{z}_h,p_h),\\ \mathcal{C}_h(p_h,w_h) &= c_0(p_h,w_h).\end{aligned}$$

Meanwhile, we define a discrete time-dependent norm on space $\mathbf{X}_h\times\mathbf{Z}_h$:

$$|||(\mathbf{v}_h,\mathbf{z}_h)|||_1=\left(|\mathbf{v}_h|_{1,h}^2+\tau^2\|\mathbf{z}_h\|_{\mathbf{H}(\mathrm{div})}^2\right)^{1/2}$$

and introduce the following kernel:

$$\begin{aligned}\operatorname{Ker}\mathcal{B}_h &= \{(\mathbf{v}_h,\mathbf{z}_h)\in\mathbf{X}_h\times\mathbf{Z}_h:\mathcal{B}_h((\mathbf{v}_h,\mathbf{z}_h),w_h)=0\quad\forall w_h\in W_h\}\\ &= \{(\mathbf{v}_h,\mathbf{z}_h)\in\mathbf{X}_h\times\mathbf{Z}_h:\alpha\mathrm{div}\,\mathbf{v}_h+\tau\mathrm{div}\,\mathbf{z}_h=0\},\qquad(3.2)\\ \operatorname{Ker}\mathcal{B}_h^T &= \{w_h\in W_h:\mathcal{B}_h((\mathbf{v}_h,\mathbf{z}_h),w_h)=0\quad\forall(\mathbf{v}_h,\mathbf{z}_h)\in\mathbf{X}_h\times\mathbf{Z}_h\}\\ &= \{0\}.\qquad(3.3)\end{aligned}$$

It is noted that the kernel of $\mathcal{B}_h$ can be directly obtained through the definitions of b_h,c_h and the fact that $\mathrm{div}_h\,\mathbf{X}_h\subseteq W_h,\mathrm{div}_h\,\mathbf{Z}_h\subseteq W_h$, while the kernel of $\mathcal{B}_h^T$ can be obtained by using the equivalent form of (2.7), more specifically, choosing $(\mathbf{v}_h,\mathbf{z}_h)\in\mathbf{X}_h\times\mathbf{Z}_h$ such that $\mathbf{v}_h=\mathbf{0},\mathrm{div}\,\mathbf{z}_h=w_h$ in the bilinear form $\mathcal{B}_h((\mathbf{v}_h,\mathbf{z}_h),w_h)=0$.

Lemma 3.1. *There exists a positive constant C, independent of h and τ, such that*

$$\mathcal{A}_h((\mathbf{v}_h,\mathbf{z}_h),(\mathbf{v}_h,\mathbf{z}_h))\geq C|||(\mathbf{v}_h,\mathbf{z}_h)|||_1^2\qquad\forall(\mathbf{v}_h,\mathbf{z}_h)\in\operatorname{Ker}\mathcal{B}_h.$$

Proof. According to (2.12), (2.14), (3.2) and Lemma 2.6, we have

$$\begin{aligned}\mathcal{A}_h((\mathbf{v}_h,\mathbf{z}_h),(\mathbf{v}_h,\mathbf{z}_h)) &\geq 2\mu\min\{1,c_*\}\|\varepsilon(\mathbf{v}_h)\|_0^2+\lambda\|\mathrm{div}\,\mathbf{v}_h\|_0^2+\tau\tilde{C}_*\left\|\kappa^{-\frac{1}{2}}\mathbf{z}_h\right\|_0^2,\\ &\geq 2\mu\min\{1,c_*\}C|\mathbf{v}_h|_{1,h}^2+\tau^2\frac{\lambda}{\alpha^2}\|\mathrm{div}\,\mathbf{z}_h\|_0^2+\tau^2\tilde{C}_*\kappa_1^{-\frac{1}{2}}\|\mathbf{z}_h\|_0^2,\end{aligned}$$

which leads to the desired result for sufficiently small $\tau>0$. □

Lemma 3.2. *There exists a positive constant C, independent of h and τ, such that*

$$\sup_{(\mathbf{v}_h,\mathbf{z}_h)\in\mathbf{X}_h\times\mathbf{Z}_h}\frac{\mathcal{B}_h((\mathbf{v}_h,\mathbf{z}_h),w_h)}{|||(\mathbf{v}_h,\mathbf{z}_h)|||_1}\geq C\|w_h\|_0\qquad\forall w_h\in W_h.$$

Proof. Taking $\mathbf{v}_h=\mathbf{0}$, it holds that

$$\frac{\mathcal{B}_h((\mathbf{v}_h,\mathbf{z}_h),w_h)}{|||(\mathbf{v}_h,\mathbf{z}_h)|||_1}=\frac{-\tau(\mathrm{div}\,\mathbf{z}_h,w_h)}{\tau\|\mathbf{z}_h\|_{\mathbf{H}(\mathrm{div})}}=\frac{\|w_h\|_0^2}{\|\mathbf{z}_h\|_{\mathbf{H}(\mathrm{div})}}\geq\tilde{\beta}\|w_h\|_0,$$

where in the second equality we use the fact that for every $w_h\in W_h$, there exists $\mathbf{z}_h\in\mathbf{Z}_h$ such that $\mathrm{div}\,\mathbf{z}_h=-w_h$ and $\tilde{\beta}\|\mathbf{z}_h\|_{\mathbf{H}(\mathrm{div})}\leq\|w_h\|_0$. □

Theorem 3.3. *The fully discrete method (2.17) has a unique solution $(\mathbf{u}_h^n,\mathbf{q}_h^n,p_h^n)\in\mathbf{X}_h\times\mathbf{Z}_h\times W_h$ at each time step t^n.*

Proof. From the positive semidefiniteness and symmetry of $\mathcal{C}_h(\cdot,\cdot)$, as well as Lemmas 3.1, 3.2 and (3.3), we can easily obtain the existence and uniqueness of a solution to (2.17). □

3.2. A unified error estimate for $c_0 \geq 0$

In order to prove optimal error estimates, we assume the following regularity conditions:

$$
\begin{aligned}
&p \in L^\infty\big(0,T;H^k(\Omega)\big) \cap L^2\big(0,T;H^k(\Omega)\big),\ p_{tt} \in L^2\big(0,T;L^2(\Omega)\big),\ \mathbf{q} \in \big[L^2\big(0,T;H^k(\Omega)\big)\big]^2,\\
&\mathbf{u} \in \big[L^\infty\big(0,T;H^{k+1}(\Omega)\big)\big]^2 \cap \big[L^2\big(0,T;H^{k+1}(\Omega)\big)\big]^2,\ \mathbf{u}_t \in \big[L^2\big(0,T;H^{k+1}(\Omega)\big)\big]^2,\ \mathbf{u}_{tt} \in \big[L^2\big(0,T;H^1(\Omega)\big)\big]^2,\\
&\mathbf{f} \in \big[L^\infty\big(0,T;H^k(\Omega)\big)\big]^2 \cap \big[L^2\big(0,T;H^k(\Omega)\big)\big]^2,\ \mathbf{f}_t \in \big[L^2\big(0,T;H^k(\Omega)\big)\big]^2,\ \mathbf{f}_{tt} \in \big[L^2\big(0,T;L^2(\Omega)\big)\big]^2. \qquad (3.4)
\end{aligned}
$$

Also, for convenience, we introduce the following notation for the time-dependent auxiliary, interpolation and projection errors:

$$
\eta_\chi^n = \chi^n - \chi_I^n, \qquad \xi_\chi^n = \chi_I^n - \chi_h^n, \qquad \zeta_\chi^n = \chi^n - \chi_\pi^n, \quad \text{with } \chi = \mathbf{u}, \mathbf{q}, \text{or } p,
$$

which leads to the fact $\chi^n - \chi_h^n = \eta_\chi^n + \xi_\chi^n$.

Theorem 3.4. *Let $(\mathbf{u},\mathbf{q},p) \in \mathbf{H}^1_{uD}(\Omega)\times\mathbf{H}_{pN}(div;\Omega)\times L^2(\Omega)$ and $(\mathbf{u}_h,\mathbf{q}_h,p_h) \in \mathbf{X}_h\times\mathbf{Z}_h\times W_h$ be, respectively, the solutions of the continuous variational problem and the fully discrete problem (2.17). If assumption (A0) holds for the family of partitions $\mathcal{T}_h$, and there is sufficient regularity (3.4) of true solutions and data functions, we have the error estimate*

$$
\max_{1\leq n\leq N}|\mathbf{u}^n - \mathbf{u}_h^n|_{1,h} + \max_{1\leq n\leq N}\|p^n - p_h^n\|_0 + \tau\sum_{n=1}^{N}\Big\|\kappa^{-\frac{1}{2}}(\mathbf{q}^n - \mathbf{q}_h^n)\Big\|_0 \leq C\big(h^k + \tau\big),
$$

where C is a constant independent of h, λ and κ.

Proof. At time $t = t^n$, multiplying equation (1.1) by the test function $(\mathbf{v}_h,\mathbf{z}_h,w_h) \in \mathbf{X}_h\times\mathbf{Z}_h\times W_h$ and using the Taylor expansion

$$
\partial_t\chi^n := \frac{\chi^n - \chi^{n-1}}{\tau} = \chi_t^n + \frac{1}{\tau}\int_{t^{n-1}}^{t^n}\big(s - t^{n-1}\big)\chi_{tt}(s)\,\mathrm{d}s, \qquad (3.5)
$$

we can obtain

$$
\begin{aligned}
\tilde{a}(\mathbf{q}^n,\mathbf{z}_h) - (p^n,\operatorname{div}\mathbf{z}_h) &= -\sum_{K\in\mathcal{T}_h}(p^n\mathbf{n}_K,\mathbf{z}_h)_{\partial K},\\
a(\mathbf{u}^n,\mathbf{v}_h) - \alpha(p^n,\operatorname{div}\mathbf{v}_h) &= (\mathbf{f}^n,\mathbf{v}_h) + \sum_{K\in\mathcal{T}_h}((\boldsymbol{\sigma}^n - \alpha p^n\boldsymbol{I})\cdot\mathbf{n}_K,\mathbf{v}_h)_{\partial K},\\
c_0(\partial_t p^n,w_h) + \alpha(\operatorname{div}\partial_t\mathbf{u}^n,w_h) + (\operatorname{div}\mathbf{q}^n,w_h) &= (g^n,w_h) + \frac{c_0}{\tau}\left(\int_{t^{n-1}}^{t^n}\big(s - t^{n-1}\big)p_{tt}(s)\,\mathrm{d}s, w_h\right)\\
&\quad + \frac{\alpha}{\tau}\left(\int_{t^{n-1}}^{t^n}\big(s - t^{n-1}\big)\operatorname{div}\mathbf{u}_{tt}(s)\,\mathrm{d}s, w_h\right). \qquad (3.6)
\end{aligned}
$$

Then, we denote the first term (corresponding to the symmetric gradient inner product) of $a_h^K(\cdot,\cdot), a^K(\cdot,\cdot)$ as $a_h^{\varepsilon,K}(\cdot,\cdot), a^{\varepsilon,K}(\cdot,\cdot)$, *i.e.*,

$$
a_h^K(\cdot,\cdot) = a_h^{\varepsilon,K}(\cdot,\cdot) + \lambda(\operatorname{div}\cdot,\operatorname{div}\cdot)_K \quad\text{and}\quad a^K(\cdot,\cdot) = a^{\varepsilon,K}(\cdot,\cdot) + \lambda(\operatorname{div}\cdot,\operatorname{div}\cdot)_K.
$$

By subtracting (2.17) from (3.6) and simplifying the resulting equations, it holds that

$$
\tilde{a}_h\big(\xi_{\mathbf{q}}^n,\mathbf{z}_h\big) - \big(\xi_p^n,\operatorname{div}\mathbf{z}_h\big) = -\sum_{K\in\mathcal{T}_h}\Big[\tilde{a}^K\big(\zeta_{\mathbf{q}}^n,\mathbf{z}_h\big) + \tilde{a}^K\Big(\mathbf{q}_\pi^n,\mathbf{z}_h - \Pi_{k-1}^{0,K}\mathbf{z}_h\Big) + \tilde{a}_h^K\big(\eta_{\mathbf{q}}^n - \zeta_{\mathbf{q}}^n,\mathbf{z}_h\big)\Big],
$$

$$a_h(\xi_{\mathbf{u}}^n,\mathbf{v}_h)-\alpha\big(\xi_p^n,\operatorname{div}\mathbf{v}_h\big)=\sum_{K\in\mathcal{T}_h}\Big[\Big(\mathbf{f}^n-\Pi_k^{0,K}\mathbf{f}^n,\mathbf{v}_h\Big)_K-a^{\varepsilon,K}(\zeta_{\mathbf{u}}^n,\mathbf{v}_h)-a_h^{\varepsilon,K}(\eta_{\mathbf{u}}^n-\zeta_{\mathbf{u}}^n,\mathbf{v}_h)$$
$$-\lambda(\operatorname{div}\eta_{\mathbf{u}}^n,\operatorname{div}\mathbf{v}_h)_K\Big]+\sum_{e\in\mathcal{E}_h^i}(\boldsymbol{\sigma}^n\cdot\mathbf{n}_e,[\![\mathbf{v}_h]\!])_e,$$
$$c_0\big(\partial_t\xi_p^n,w_h\big)+\alpha(\operatorname{div}\partial_t\xi_{\mathbf{u}}^n,w_h)+\big(\operatorname{div}\xi_{\mathbf{q}}^n,w_h\big)=\frac{c_0}{\tau}\left(\int_{t^{n-1}}^{t^n}(s-t^{n-1})p_{tt}(s)\,\mathrm{d}s,w_h\right)$$
$$+\frac{\alpha}{\tau}\left(\int_{t^{n-1}}^{t^n}(s-t^{n-1})\operatorname{div}\mathbf{u}_{tt}(s)\,\mathrm{d}s,w_h\right),\tag{3.7}$$

where we use the k-consistency (2.13), the boundary conditions (1.1d) and (1.1e), the continuity of $\mathbf{v}_h\cdot\mathbf{n}_e$ and $\mathbf{z}_h\cdot\mathbf{n}_e$ on each edge $e\in\mathcal{E}_h^i$, and the fact from (2.5) and (2.8):

$$\big(\eta_p^n,w_h\big)_K=0,\quad\big(\eta_p^n,\operatorname{div}\mathbf{z}_h\big)_K=0,\quad\big(\eta_p^n,\operatorname{div}\mathbf{v}_h\big)_K=0,$$
$$\big(\operatorname{div}\eta_{\mathbf{q}}^n,w_h\big)_K=0,\quad(\operatorname{div}\eta_{\mathbf{u}}^n,w_h)_K=0.$$

Now, taking $\mathbf{v}_h=\xi_{\mathbf{u}}^n-\xi_{\mathbf{u}}^{n-1},\mathbf{z}_h=\tau\xi_{\mathbf{q}}^n,w_h=\tau\xi_p^n$ in (3.7), adding the resulting equations, using the following inequalities

$$a_h\big(\xi_{\mathbf{u}}^n,\xi_{\mathbf{u}}^n-\xi_{\mathbf{u}}^{n-1}\big)\geq\frac{1}{2}a_h(\xi_{\mathbf{u}}^n,\xi_{\mathbf{u}}^n)-\frac{1}{2}a_h\big(\xi_{\mathbf{u}}^{n-1},\xi_{\mathbf{u}}^{n-1}\big),$$
$$c_0\big(\xi_p^n,\xi_p^n-\xi_p^{n-1}\big)\geq\frac{c_0}{2}\|\xi_p^n\|_0^2-\frac{c_0}{2}\|\xi_p^{n-1}\|_0^2,$$

and summing from 1 to N, we see that

$$\frac{1}{2}a_h\big(\xi_{\mathbf{u}}^N,\xi_{\mathbf{u}}^N\big)-\frac{1}{2}a_h\big(\xi_{\mathbf{u}}^0,\xi_{\mathbf{u}}^0\big)+\frac{c_0}{2}\|\xi_p^N\|_0^2-\frac{c_0}{2}\|\xi_p^0\|_0^2+\tau\sum_{n=1}^N\tilde{a}_h\big(\xi_{\mathbf{q}}^n,\xi_{\mathbf{q}}^n\big)$$
$$\leq\underbrace{-\tau\sum_{n=1}^N\sum_{K\in\mathcal{T}_h}\Big[\tilde{a}^K\big(\zeta_{\mathbf{q}}^n,\xi_{\mathbf{q}}^n\big)+\tilde{a}^K\Big(\mathbf{q}_\pi^n,\xi_{\mathbf{q}}^n-\Pi_{k-1}^{0,K}\xi_{\mathbf{q}}^n\Big)+\tilde{a}_h^K\big(\eta_{\mathbf{q}}^n-\zeta_{\mathbf{q}}^n,\xi_{\mathbf{q}}^n\big)\Big]}_{\Phi_1}$$
$$+\underbrace{\sum_{n=1}^N\sum_{K\in\mathcal{T}_h}\Big[\Big(\mathbf{f}^n-\Pi_k^{0,K}\mathbf{f}^n,\xi_{\mathbf{u}}^n-\xi_{\mathbf{u}}^{n-1}\Big)_K-a^{\varepsilon,K}\big(\zeta_{\mathbf{u}}^n,\xi_{\mathbf{u}}^n-\xi_{\mathbf{u}}^{n-1}\big)-a_h^{\varepsilon,K}\big(\eta_{\mathbf{u}}^n-\zeta_{\mathbf{u}}^n,\xi_{\mathbf{u}}^n-\xi_{\mathbf{u}}^{n-1}\big)}_{\Phi_2}$$
$$\underbrace{-\lambda\big(\operatorname{div}\eta_{\mathbf{u}}^n,\operatorname{div}\big(\xi_{\mathbf{u}}^n-\xi_{\mathbf{u}}^{n-1}\big)\big)_K\Big]}_{\Phi_2}$$
$$+\underbrace{\sum_{n=1}^N\sum_{e\in\mathcal{E}_h^i}\big(\boldsymbol{\sigma}^n\cdot\mathbf{n}_e,[\![\xi_{\mathbf{u}}^n-\xi_{\mathbf{u}}^{n-1}]\!]\big)_e}_{\Phi_3}$$
$$+\underbrace{c_0\sum_{n=1}^N\left(\int_{t^{n-1}}^{t^n}(s-t^{n-1})p_{tt}(s)\,\mathrm{d}s,\xi_p^n\right)+\alpha\sum_{n=1}^N\left(\int_{t^{n-1}}^{t^n}(s-t^{n-1})\operatorname{div}\mathbf{u}_{tt}(s)\,\mathrm{d}s,\xi_p^n\right)}_{\Phi_4}.$$

That is, according to (2.12), (2.14), Lemma 2.6 and the fact $\xi_{\mathbf{u}}^0=\mathbf{0},\xi_p^0=0$, it is easy to get the following inequality:

$$\frac{C_*}{2}|\xi_{\mathbf{u}}^N|_{1,h}^2+\frac{c_0}{2}\|\xi_p^N\|_0^2+\tilde{C}_*\tau\sum_{n=1}^N\Big\|\kappa^{-\frac{1}{2}}\xi_{\mathbf{q}}^n\Big\|_0^2\leq\Phi_1+\Phi_2+\Phi_3+\Phi_4.\tag{3.8}$$

First, we apply Cauchy–Schwarz's and Young's inequalities to bound Φ_1:

$$\begin{aligned}\Phi_1 &= -\tau\sum_{n=1}^{N}\sum_{K\in\mathcal{T}_h}\Big[\tilde{a}^K\big(\zeta_{\mathbf{q}}^n,\xi_{\mathbf{q}}^n\big)+\Big(\kappa^{-1}\mathbf{q}_\pi^n-\Pi_{k-1}^{0,K}\big(\kappa^{-1}\mathbf{q}_\pi^n\big),\xi_{\mathbf{q}}^n\Big)+\tilde{a}_h^K\big(\eta_{\mathbf{q}}^n-\zeta_{\mathbf{q}}^n,\xi_{\mathbf{q}}^n\big)\Big]\\ &\le \tau\sum_{n=1}^{N}\sum_{K\in\mathcal{T}_h}\Big[\Big\|\kappa^{-\frac{1}{2}}\zeta_{\mathbf{q}}^n\Big\|_{0,K}\Big\|\kappa^{-\frac{1}{2}}\xi_{\mathbf{q}}^n\Big\|_{0,K}+\Big\|\kappa^{\frac{1}{2}}\Big(\kappa^{-1}\mathbf{q}_\pi^n-\Pi_{k-1}^{0,K}\big(\kappa^{-1}\mathbf{q}_\pi^n\big)\Big)\|_{0,K}\Big\|\kappa^{-\frac{1}{2}}\xi_{\mathbf{q}}^n\Big\|_{0,K}\\ &\quad+\tilde{C}^*\Big(\Big\|\kappa^{-\frac{1}{2}}\eta_{\mathbf{q}}^n\Big\|_{0,K}+\Big\|\kappa^{-\frac{1}{2}}\zeta_{\mathbf{q}}^n\Big\|_{0,K}\Big)\Big\|\kappa^{-\frac{1}{2}}\xi_{\mathbf{q}}^n\Big\|_{0,K}\Big]\\ &\le 3\varepsilon_1\tau\sum_{n=1}^{N}\Big\|\kappa^{-\frac{1}{2}}\xi_{\mathbf{q}}^n\Big\|_0^2+C\tau\sum_{n=0}^{N}\Big[\big\|\zeta_{\mathbf{q}}^n\big\|_0^2+\big\|\eta_{\mathbf{q}}^n\big\|_0^2+h^{2k}\|\mathbf{q}^n\|_k^2\Big].\end{aligned}$$

To estimate Φ_2, we need to use the Taylor expansion (3.5) and the following discrete integration by parts formula for the grid functions χ^n and ψ^n:

$$\sum_{n=1}^{N}\mathcal{A}\big(\chi^n,\psi^n-\psi^{n-1}\big)=\mathcal{A}\big(\chi^N,\psi^N\big)-\mathcal{A}\big(\chi^0,\psi^0\big)-\sum_{n=1}^{N}\mathcal{A}\big(\chi^n-\chi^{n-1},\psi^{n-1}\big). \tag{3.9}$$

Taking the second term in Φ_2 as an example, we have

$$\begin{aligned}\sum_{n=1}^{N}\sum_{K\in\mathcal{T}_h}a^{\varepsilon,K}\big(\zeta_{\mathbf{u}}^n,\xi_{\mathbf{u}}^n-\xi_{\mathbf{u}}^{n-1}\big)&=\sum_{K\in\mathcal{T}_h}\Big[a^{\varepsilon,K}\big(\zeta_{\mathbf{u}}^N,\xi_{\mathbf{u}}^N\big)-\sum_{n=1}^{N}a^{\varepsilon,K}\big(\zeta_{\mathbf{u}}^n-\zeta_{\mathbf{u}}^{n-1},\xi_{\mathbf{u}}^{n-1}\big)\Big]\\ &=\sum_{K\in\mathcal{T}_h}\Big[a^{\varepsilon,K}\big(\zeta_{\mathbf{u}}^N,\xi_{\mathbf{u}}^N\big)-\sum_{n=1}^{N}a^{\varepsilon,K}\big(\tau\zeta_{\mathbf{u}t}^n,\xi_{\mathbf{u}}^{n-1}\big)-\sum_{n=1}^{N}a^{\varepsilon,K}\Big(\int_{t^{n-1}}^{t^n}(s-t^{n-1})\zeta_{\mathbf{u}tt}(s)\,\mathrm{d}s,\xi_{\mathbf{u}}^{n-1}\Big)\Big]\\ &\le\big\|\zeta_{\mathbf{u}}^N\big\|_1\big|\xi_{\mathbf{u}}^N\big|_{1,h}+\tau\sum_{n=1}^{N}\|\zeta_{\mathbf{u}t}^n\|_1\big|\xi_{\mathbf{u}}^{n-1}\big|_{1,h}+\sum_{n=1}^{N}\tau^{\frac{3}{2}}\Big(\int_{t^{n-1}}^{t^n}\|\zeta_{\mathbf{u}tt}\|_1^2\,\mathrm{d}s\Big)^{\frac{1}{2}}\big|\xi_{\mathbf{u}}^{n-1}\big|_{1,h}\\ &\le\varepsilon_2|\xi_{\mathbf{u}}^N|_{1,h}^2+C\Big[\big\|\zeta_{\mathbf{u}}^N\big\|_1^2+\tau\sum_{n=0}^{N}\Big(\|\zeta_{\mathbf{u}t}^n\|_1^2+|\xi_{\mathbf{u}}^n|_{1,h}^2\Big)+\tau^2\int_0^T\|\zeta_{\mathbf{u}tt}\|_1^2\,\mathrm{d}s\Big],\end{aligned}$$

where in the third equality we use the estimate with different norms $\|\cdot\|_\Upsilon$:

$$\Big\|\int_{t^{n-1}}^{t^n}(s-t^{n-1})\chi(s)\,\mathrm{d}s\Big\|_\Upsilon\le\tau^{\frac{3}{2}}\Big(\int_{t^{n-1}}^{t^n}\|\chi\|_\Upsilon^2\,\mathrm{d}s\Big)^{\frac{1}{2}}. \tag{3.10}$$

Similarly, we can derive the estimations of the residual terms in Φ_2 and give the following result:

$$\begin{aligned}\Phi_2&\le 4\varepsilon_2|\xi_{\mathbf{u}}^N|_{1,h}^2+C\Big[\tau\sum_{n=0}^{N}\Big(\|\zeta_{\mathbf{u}t}^n\|_1^2+|\eta_{\mathbf{u}t}^n|_{1,h}^2+\|\lambda\mathrm{div}\,\eta_{\mathbf{u}t}^n\|_0^2+\Big\|\mathbf{f}_t^n-\Pi_k^{0,K}\mathbf{f}_t^n\Big\|_0^2+|\xi_{\mathbf{u}}^n|_{1,h}^2\Big)+\big\|\zeta_{\mathbf{u}}^N\big\|_1^2+\big|\eta_{\mathbf{u}}^N\big|_{1,h}^2\\ &\quad+\big\|\lambda\mathrm{div}\,\eta_{\mathbf{u}}^N\big\|_0^2+\Big\|\mathbf{f}^N-\Pi_k^{0,K}\mathbf{f}^N\Big\|_0^2+\tau^2\int_0^T\|\zeta_{\mathbf{u}tt}\|_1^2+|\eta_{\mathbf{u}tt}|_{1,h}^2+\|\lambda\mathrm{div}\,\eta_{\mathbf{u}tt}\|_0^2+\Big\|\mathbf{f}_{tt}-\Pi_k^{0,K}\mathbf{f}_{tt}\Big\|_0^2\,\mathrm{d}s\Big]\\ &\le 4\varepsilon_2\big|\xi_{\mathbf{u}}^N\big|_{1,h}^2+C\Big[\tau\sum_{n=0}^{N}\Big(\|\zeta_{\mathbf{u}t}^n\|_1^2+|\eta_{\mathbf{u}t}^n|_{1,h}^2+\|\lambda\mathrm{div}\,\eta_{\mathbf{u}t}^n\|_0^2+|\xi_{\mathbf{u}}^n|_{1,h}^2+h^{2k}\|\mathbf{f}_t^n\|_k^2\Big)+\big\|\zeta_{\mathbf{u}}^N\big\|_1^2+\big|\eta_{\mathbf{u}}^N\big|_{1,h}^2\\ &\quad+\big\|\lambda\mathrm{div}\,\eta_{\mathbf{u}}^N\big\|_0^2+h^{2k}\big\|\mathbf{f}^N\big\|_k^2+\tau^2\int_0^T\|\zeta_{\mathbf{u}tt}\|_1^2+|\eta_{\mathbf{u}tt}|_{1,h}^2+\|\lambda\mathrm{div}\,\eta_{\mathbf{u}tt}\|_0^2+\|\mathbf{f}_{tt}\|_0^2\,\mathrm{d}s\Big].\end{aligned}$$

Next, we apply the discrete integration by parts formula (3.9), another Taylor expansion and its estimate

$$\left\|\chi^n-\chi^{n-1}\right\|_k=\left\|\int_{t^{n-1}}^{t^n}\chi_t(s)\,\mathrm{d}s\right\|_k\le\tau^{\frac12}\left(\int_{t^{n-1}}^{t^n}\|\chi_t\|_k^2\,\mathrm{d}s\right)^{\frac12}$$

to get

$$\begin{aligned}
\Phi_3&=\sum_{n=1}^{N}\left[\sum_{K\in\mathcal{T}_h}\left(\boldsymbol{\sigma}^n\cdot\mathbf{n}_K,\xi_{\mathbf{u}}^n-\xi_{\mathbf{u}}^{n-1}\right)_{\partial K}-\sum_{e\in\mathcal{E}_h^b}\left(\boldsymbol{\sigma}^n\cdot\mathbf{n}_e,\xi_{\mathbf{u}}^n-\xi_{\mathbf{u}}^{n-1}\right)_e\right]\\
&=\sum_{K\in\mathcal{T}_h}\left[\left(\boldsymbol{\sigma}^N\cdot\mathbf{n}_K,\xi_{\mathbf{u}}^N\right)_{\partial K}-\sum_{n=1}^{N}\left(\left(\boldsymbol{\sigma}^n-\boldsymbol{\sigma}^{n-1}\right)\cdot\mathbf{n}_K,\xi_{\mathbf{u}}^{n-1}\right)_{\partial K}\right]\\
&\quad-\sum_{e\in\mathcal{E}_h^b}\left[\left(\boldsymbol{\sigma}^N\cdot\mathbf{n}_e,\xi_{\mathbf{u}}^N\right)_e-\sum_{n=1}^{N}\left(\left(\boldsymbol{\sigma}^n-\boldsymbol{\sigma}^{n-1}\right)\cdot\mathbf{n}_e,\xi_{\mathbf{u}}^{n-1}\right)_e\right]\\
&=\sum_{e\in\mathcal{E}_h^i}\left[\left(\left[\!\left[\xi_{\mathbf{u}}^N\cdot\mathbf{t}_e\right]\!\right],\left(\boldsymbol{\sigma}^N\right)^T:\left(\mathbf{n}_e\otimes\mathbf{t}_e\right)\right)_e-\sum_{n=1}^{N}\left(\left[\!\left[\xi_{\mathbf{u}}^{n-1}\cdot\mathbf{t}_e\right]\!\right],\left(\boldsymbol{\sigma}^n-\boldsymbol{\sigma}^{n-1}\right)^T:\left(\mathbf{n}_e\otimes\mathbf{t}_e\right)\right)_e\right]\\
&=\sum_{e\in\mathcal{E}_h^i}\left[\left(\left[\!\left[\xi_{\mathbf{u}}^N\cdot\mathbf{t}_e\right]\!\right]-\Pi_0^{0,e}\left[\!\left[\xi_{\mathbf{u}}^N\cdot\mathbf{t}_e\right]\!\right],\left(\boldsymbol{\sigma}^N\right)^T:\left(\mathbf{n}_e\otimes\mathbf{t}_e\right)-\Pi_{k-1}^{0,e}\left(\left(\boldsymbol{\sigma}^N\right)^T:\left(\mathbf{n}_e\otimes\mathbf{t}_e\right)\right)\right)_e\right.\\
&\quad\left.-\sum_{n=1}^{N}\left(\left[\!\left[\xi_{\mathbf{u}}^{n-1}\cdot\mathbf{t}_e\right]\!\right]-\Pi_0^{0,e}\left[\!\left[\xi_{\mathbf{u}}^{n-1}\cdot\mathbf{t}_e\right]\!\right],\left(\boldsymbol{\sigma}^n-\boldsymbol{\sigma}^{n-1}\right)^T:\left(\mathbf{n}_e\otimes\mathbf{t}_e\right)-\Pi_{k-1}^{0,e}\left(\left(\boldsymbol{\sigma}^n-\boldsymbol{\sigma}^{n-1}\right)^T:\left(\mathbf{n}_e\otimes\mathbf{t}_e\right)\right)\right)_e\right]\\
&\le Ch^k\left|\xi_{\mathbf{u}}^N\right|_{1,h}\left\|\boldsymbol{\sigma}^N\right\|_k+C\sum_{n=1}^{N}h^k\tau^{\frac12}\left|\xi_{\mathbf{u}}^{n-1}\right|_{1,h}\left(\int_{t^{n-1}}^{t^n}\|\boldsymbol{\sigma}_t\|_k^2\,\mathrm{d}s\right)^{\frac12}\\
&\le\varepsilon_3\left|\xi_{\mathbf{u}}^N\right|_{1,h}^2+C\left[h^{2k}\left\|\mathbf{u}^N\right\|_{k+1}^2+\tau\sum_{n=0}^{N}|\xi_{\mathbf{u}}^n|_{1,h}^2+h^{2k}\int_0^T\|\mathbf{u}_t\|_{k+1}^2\,\mathrm{d}s\right],
\end{aligned}$$

where in the third equality we use the equivalent deformation of the boundary term:

$$\begin{aligned}
\sum_{K\in\mathcal{T}_h}(\boldsymbol{\chi},\Psi\cdot\mathbf{n}_K)_{\partial K}&=\sum_{K\in\mathcal{T}_h}\left(\boldsymbol{\chi}\cdot\mathbf{n}_K,\Psi^T:(\mathbf{n}_K\otimes\mathbf{n}_K)\right)_{\partial K}+\sum_{K\in\mathcal{T}_h}\left(\boldsymbol{\chi}\cdot\mathbf{t}_K,\Psi^T:(\mathbf{n}_K\otimes\mathbf{t}_K)\right)_{\partial K}\\
&=\sum_{e\in\mathcal{E}_h}\left(\boldsymbol{\chi}\cdot\mathbf{n}_e,\left[\!\left[\Psi^T:(\mathbf{n}_e\otimes\mathbf{n}_e)\right]\!\right]\right)_e+\sum_{e\in\mathcal{E}_h}\left(\left[\!\left[\boldsymbol{\chi}\cdot\mathbf{t}_e\right]\!\right],\Psi^T:(\mathbf{n}_e\otimes\mathbf{t}_e)\right)_e
\end{aligned}$$

and the continuity of $\xi_{\mathbf{u}}^n\cdot\mathbf{n}_e$ on each edge $e\in\mathcal{E}_h^i$.

Then, we are in a position to bound Φ_4. Combining (3.10) with Cauchy–Schwarz's and Young's inequalities, it is easy to derive at

$$\begin{aligned}
\Phi_4&\le c_0\sum_{n=1}^{N}\left\|\int_{t^{n-1}}^{t^n}(s-t^{n-1})p_{tt}(s)\,\mathrm{d}s\right\|_0\|\xi_p^n\|_0+\alpha\sum_{n=1}^{N}\left\|\int_{t^{n-1}}^{t^n}(s-t^{n-1})\mathrm{div}\,\mathbf{u}_{tt}(s)\,\mathrm{d}s\right\|_0\|\xi_p^n\|_0\\
&\le\sum_{n=1}^{N}c_0\tau^{\frac32}\left(\int_{t^{n-1}}^{t^n}\|p_{tt}\|_0^2\,\mathrm{d}s\right)^{\frac12}\|\xi_p^n\|_0+\sum_{n=1}^{N}\alpha\tau^{\frac32}\left(\int_{t^{n-1}}^{t^n}\|\mathrm{div}\,\mathbf{u}_{tt}\|_0^2\,\mathrm{d}s\right)^{\frac12}\|\xi_p^n\|_0\\
&\le C\tau\sum_{n=0}^{N}\|\xi_p^n\|_0^2+C\tau^2\int_0^T c_0\|p_{tt}\|_0^2+\|\mathbf{u}_{tt}\|_1^2\,\mathrm{d}s.
\end{aligned}$$

Obviously, for $c_0 > 0$, from (3.8) and the estimations of $\Phi_1 - \Phi_4$, we see that

$$\begin{aligned}
&\Big(\frac{C_*}{2} - 4\varepsilon_2 - \varepsilon_3\Big)|\xi_{\mathbf{u}}^N|_{1,h}^2 + \frac{c_0}{2}\|\xi_p^N\|_0^2 + \big(\tilde{C}_* - 3\varepsilon_1\big)\tau\sum_{n=1}^{N}\Big\|\kappa^{-\frac{1}{2}}\xi_{\mathbf{q}}^n\Big\|_0^2 \\
&\quad\le C\Bigg[\tau\sum_{n=0}^{N}\Big(|\xi_{\mathbf{u}}^n|_{1,h}^2 + \|\xi_p^n\|_0^2\Big) + \|\zeta_{\mathbf{u}}^N\|_1^2 + |\eta_{\mathbf{u}}^N|_{1,h}^2 + \|\lambda\mathrm{div}\,\eta_{\mathbf{u}}^N\|_0^2 + h^{2k}\|\mathbf{f}^N\|_k^2 + h^{2k}\|\mathbf{u}^N\|_{k+1}^2 \\
&\qquad + \tau\sum_{n=0}^{N}\Big(\|\zeta_{\mathbf{q}}^n\|_0^2 + \|\zeta_{\mathbf{u}t}^n\|_1^2 + \|\eta_{\mathbf{q}}^n\|_0^2 + |\eta_{\mathbf{u}t}^n|_{1,h}^2 + \|\lambda\mathrm{div}\,\eta_{\mathbf{u}t}^n\|_0^2 + h^{2k}\|\mathbf{q}^n\|_k^2 + h^{2k}\|\mathbf{f}_t^n\|_k^2\Big) \\
&\qquad + h^{2k}\int_0^T\|\mathbf{u}_t\|_{k+1}^2\,\mathrm{d}s + \tau^2\int_0^T\|\zeta_{\mathbf{u}tt}\|_1^2 + |\eta_{\mathbf{u}tt}|_{1,h}^2 + \|\lambda\mathrm{div}\,\eta_{\mathbf{u}tt}\|_0^2 + \|\mathbf{f}_{tt}\|_0^2 + \|p_{tt}\|_0^2 + \|\mathbf{u}_{tt}\|_1^2\,\mathrm{d}s\Bigg],
\end{aligned} \tag{3.11}$$

which leads to

$$\max_{1\le n\le N}|\xi_{\mathbf{u}}^n|_{1,h}^2 + \max_{1\le n\le N}\|\xi_p^n\|_0^2 + \tau\sum_{n=1}^{N}\Big\|\kappa^{-\frac{1}{2}}\xi_{\mathbf{q}}^n\Big\|_0^2 \le C\big(h^{2k} + \tau^2\big)$$

for sufficiently small $\varepsilon_1, \varepsilon_2, \varepsilon_3$ by using the discrete Gronwall's lemma, the appropriate interpolation and projection errors (2.5), (2.6), (2.9), and the fact that $\|\lambda\mathrm{div}\,\mathbf{u}\|_k, \|\lambda\mathrm{div}\,\mathbf{u}_t\|_k, \|\lambda\mathrm{div}\,\mathbf{u}_{tt}\|_k$ can be bounded by a constant related to the right-hand term $\mathbf{f}, g$ and the initial condition (*cf.* Thm. 3.3 in [26]). For $c_0 = 0$, according to (2.10) and (3.7), we need to consider

$$\begin{aligned}
\|\xi_p^n\|_0 &\le \frac{1}{\beta}\frac{(\mathrm{div}\,\mathbf{v}_h, \xi_p^n)}{|\mathbf{v}_h|_{1,h}} \\
&= \frac{1}{\alpha\beta|\mathbf{v}_h|_{1,h}}\Bigg\{\sum_{K\in\mathcal{T}_h}\Big[a_h^K(\xi_{\mathbf{u}}^n, \mathbf{v}_h) - \Big(\mathbf{f}^n - \Pi_k^{0,K}\mathbf{f}^n, \mathbf{v}_h\Big)_K + a^{\varepsilon,K}(\zeta_{\mathbf{u}}^n, \mathbf{v}_h) + a_h^{\varepsilon,K}(\eta_{\mathbf{u}}^n - \zeta_{\mathbf{u}}^n, \mathbf{v}_h) \\
&\quad + \lambda(\mathrm{div}\,\eta_{\mathbf{u}}^n, \mathrm{div}\,\mathbf{v}_h)_K\Big] + \sum_{e\in\mathcal{E}_h^i}(\boldsymbol{\sigma}^n\cdot\mathbf{n}_e, [\![\mathbf{v}_h]\!])_e\Bigg\} \\
&\le C\Big[|\xi_{\mathbf{u}}^n|_{1,h} + \|\zeta_{\mathbf{u}}^n\|_1 + |\eta_{\mathbf{u}}^n|_{1,h} + \|\lambda\mathrm{div}\,\eta_{\mathbf{u}}^n\|_0 + h^k\|\mathbf{f}^n\|_k + h^k\|\boldsymbol{\sigma}^n\|_k\Big].
\end{aligned} \tag{3.12}$$

That is, we have the following formula instead of (3.11):

$$\begin{aligned}
&\Big(\frac{C_*}{2} - 4\varepsilon_2 - \varepsilon_3\Big)|\xi_{\mathbf{u}}^N|_{1,h}^2 + \big(\tilde{C}_* - 3\varepsilon_1\big)\tau\sum_{n=1}^{N}\Big\|\kappa^{-\frac{1}{2}}\xi_{\mathbf{q}}^n\Big\|_0^2 \\
&\quad\le C\Bigg[\tau\sum_{n=0}^{N}|\xi_{\mathbf{u}}^n|_{1,h}^2 + \|\zeta_{\mathbf{u}}^N\|_1^2 + |\eta_{\mathbf{u}}^N|_{1,h}^2 + \|\lambda\mathrm{div}\,\eta_{\mathbf{u}}^N\|_0^2 + h^{2k}\|\mathbf{f}^N\|_k^2 + h^{2k}\|\mathbf{u}^N\|_{k+1}^2 + \tau\sum_{n=0}^{N}\Big(\|\zeta_{\mathbf{q}}^n\|_0^2 + \|\zeta_{\mathbf{u}}^n\|_1^2 \\
&\qquad + \|\zeta_{\mathbf{u}t}^n\|_1^2 + \|\eta_{\mathbf{q}}^n\|_0^2 + |\eta_{\mathbf{u}}^n|_{1,h}^2 + |\eta_{\mathbf{u}t}^n|_{1,h}^2 + \|\lambda\mathrm{div}\,\eta_{\mathbf{u}}^n\|_0^2 + \|\lambda\mathrm{div}\,\eta_{\mathbf{u}t}^n\|_0^2 + h^{2k}\|\mathbf{q}^n\|_k^2 + h^{2k}\|\mathbf{u}^n\|_{k+1}^2 + h^{2k}\|\mathbf{f}^n\|_k^2 \\
&\qquad + h^{2k}\|\mathbf{f}_t^n\|_k^2\Big) + h^{2k}\int_0^T\|\mathbf{u}_t\|_{k+1}^2\,\mathrm{d}s + \tau^2\int_0^T\|\zeta_{\mathbf{u}tt}\|_1^2 + |\eta_{\mathbf{u}tt}|_{1,h}^2 + \|\lambda\mathrm{div}\,\eta_{\mathbf{u}tt}\|_0^2 + \|\mathbf{f}_{tt}\|_0^2 + \|\mathbf{u}_{tt}\|_1^2\,\mathrm{d}s\Bigg],
\end{aligned}$$

which means that

$$\max_{1\le n\le N}|\xi_{\mathbf{u}}^n|_{1,h}^2 + \tau\sum_{n=1}^{N}\Big\|\kappa^{-\frac{1}{2}}\xi_{\mathbf{q}}^n\Big\|_0^2 \le C\big(h^{2k} + \tau^2\big).$$

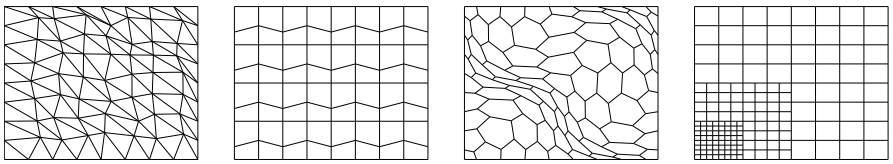

FIGURE 1. Sample meshes: from *left* $\mathcal{T}_h^1$ to *right* $\mathcal{T}_h^4$ for $h = 1/8$.

Finally, combined with (3.12), it is clear that

$$\max_{1\le n\le N}\left\|\xi_p^n\right\|_0^2 \le C\big(h^{2k}+\tau^2\big).$$

□

4. Numerical experiments

In this section, we test two poroelasticity problems to validate the accuracy and effectiveness of our proposed virtual element method. The first example is used to confirm the optimal convergence rates with different approximation accuracy and different meshes, and to illustrate that our method is Poisson-locking-free by comparing with a coupled continuous-mixed virtual element method. The second example is used to verify that our method overcomes spurious pressure oscillations by testing the cantilever bracket problem and the Barry and Mercer problem.

Firstly, we give the following diagram of mesh partitions, *i.e.*, randomly distorted triangular mesh $\mathcal{T}_h^1$, uniform trapezoidal mesh $\mathcal{T}_h^2$, non-structured hexagonal mesh $\mathcal{T}_h^3$, and hanging-node mesh $\mathcal{T}_h^4$, in Figure 1. Also, we introduce the error measures by

$$\begin{aligned}
\mathrm{err}_{\mathbf{u}} &:= \sqrt{\sum_{K\in\mathcal{T}_h} a_h^K\big(\mathbf{u}_h^N-\mathbf{u}_I^N,\mathbf{u}_h^N-\mathbf{u}_I^N\big)} && \text{for the displacement,}\\
\mathrm{err}_p &:= \left\|p^N-p_h^N\right\|_0 && \text{for the pressure,}\\
\mathrm{err}_{\mathbf{q}} &:= \left(\tau\sum_{n=1}^{N}\|\mathbf{q}^n-\Pi_{k-1}^{0,K}\mathbf{q}_h^n\|_0^2\right)^{1/2} && \text{for the fluid velocity,}
\end{aligned}$$

and use the classical stability formulas for every $\mathbf{u}_h,\mathbf{v}_h\in\mathbf{X}_h$ and $\mathbf{q}_h,\mathbf{z}_h\in\mathbf{Z}_h$

$$S^K(\mathbf{u}_h,\mathbf{v}_h)=\sum_{r=1}^{\dim\mathbf{X}_{h|K}}\varrho_r^{\mathbf{X}}(\mathbf{u}_h)\varrho_r^{\mathbf{X}}(\mathbf{v}_h),\qquad \widetilde{S}^K(\mathbf{q}_h,\mathbf{z}_h)=\kappa^{-1}|K|\sum_{r=1}^{\dim\mathbf{Z}_{h|K}}\varrho_r^{\mathbf{Z}}(\mathbf{q}_h)\varrho_r^{\mathbf{Z}}(\mathbf{z}_h).$$

4.1. Convergence and Poisson-locking test

We give the physical parameters $\alpha=1,\kappa=1,\mu=1,\lambda=10^8$ and choose the following exact solution on domain $\Omega:=[0,1]^2$ with $T=1$:

$$\mathbf{u}=\begin{bmatrix} e^{-t}\Big(\sin(2\pi y)(\cos(2\pi x)-1)+\frac{1}{\mu+\lambda}\sin(\pi x)\sin(\pi y)\Big)\\ e^{-t}\Big(\sin(2\pi x)(1-\cos(2\pi y))+\frac{1}{\mu+\lambda}\sin(\pi x)\sin(\pi y)\Big)\end{bmatrix},\qquad p=e^{-t}\sin(\pi x)\sin(\pi y),$$

which helps us determine the values of the right-hand terms $\mathbf{f},g$ and impose the Dirichlet boundary conditions for $\mathbf{u},p$. It should be noted that the solution satisfies $\operatorname{div}\mathbf{u}\to 0$ as $\lambda\to\infty$ at any time t.

TABLE 1. Error results of our method on $\mathcal{T}_h^1$, $\mathcal{T}_h^2$, $\mathcal{T}_h^3$ and $\mathcal{T}_h^4$ for $k = 1, c_0 = 0$.

Mesh	h	$\text{err}_{\mathbf{u}}$	Rate	$\text{err}_{\mathbf{q}}$	Rate	err_p	Rate
$\mathcal{T}_h^1$	1/8	2.2397e+00	–	1.1906e−01	–	2.4081e−02	–
	1/16	1.2117e+00	0.89	5.9733e−02	1.00	1.2040e−02	1.00
	1/32	6.2103e−01	0.96	2.9892e−02	1.00	6.0195e−03	1.00
	1/64	3.1261e−01	0.99	1.4949e−02	1.00	3.0097e−03	1.00
$\mathcal{T}_h^2$	1/8	5.5992e−01	–	1.3068e−01	–	2.9669e−02	–
	1/16	1.9654e−01	1.51	6.5466e−02	1.00	1.4770e−02	1.01
	1/32	8.2191e−02	1.26	3.2749e−02	1.00	7.3755e−03	1.00
	1/64	3.8683e−02	1.09	1.6376e−02	1.00	3.6865e−03	1.00
$\mathcal{T}_h^3$	1/8	4.4401e+00	–	1.5355e−01	–	3.2977e−02	–
	1/16	1.8703e+00	1.25	8.1024e−02	0.92	1.7160e−02	0.94
	1/32	7.6462e−01	1.29	4.2535e−02	0.93	8.7301e−03	0.97
	1/64	2.9228e−01	1.39	2.2662e−02	0.91	4.4063e−03	0.99
$\mathcal{T}_h^4$	1/8	5.4108e−01	–	1.1741e−01	–	2.6607e−02	–
	1/16	1.9393e−01	1.48	5.8830e−02	1.00	1.3253e−02	1.00
	1/32	7.9461e−02	1.29	2.9438e−02	1.00	6.6192e−03	1.00
	1/64	3.6268e−02	1.13	1.4724e−02	1.00	3.3087e−03	1.00

TABLE 2. Error results of our method on $\mathcal{T}_h^1$, $\mathcal{T}_h^2$, $\mathcal{T}_h^3$ and $\mathcal{T}_h^4$ for $k = 2, c_0 = 0$.

Mesh	h	$\text{err}_{\mathbf{u}}$	Rate	$\text{err}_{\mathbf{q}}$	Rate	err_p	Rate
$\mathcal{T}_h^1$	1/8	2.7884e−01	–	9.1036e−03	–	1.8225e−03	–
	1/16	7.2517e−02	1.94	2.3044e−03	1.98	4.5724e−04	1.99
	1/32	1.8578e−02	1.96	5.7792e−04	2.00	1.1441e−04	2.00
	1/64	4.7116e−03	1.98	1.4459e−04	2.00	2.8607e−05	2.00
$\mathcal{T}_h^2$	1/8	9.4919e−02	–	1.2410e−02	–	2.7805e−03	–
	1/16	2.4156e−02	1.97	3.1045e−03	2.00	6.9819e−04	1.99
	1/32	6.0655e−03	1.99	7.7650e−04	2.00	1.7474e−04	2.00
	1/64	1.5194e−03	2.00	1.9415e−04	2.00	4.3698e−05	2.00
$\mathcal{T}_h^3$	1/8	4.3476e+00	–	2.5341e−02	–	1.0555e−02	–
	1/16	1.0050e+00	2.11	5.9272e−03	2.10	1.7922e−03	2.56
	1/32	2.3419e−01	2.10	1.4517e−03	2.03	3.2530e−04	2.46
	1/64	5.3947e−02	2.12	3.1030e−04	2.23	5.9658e−05	2.45
$\mathcal{T}_h^4$	1/8	1.0249e−01	–	1.0890e−02	–	2.4215e−03	–
	1/16	2.3543e−02	2.12	2.7171e−03	2.00	6.0806e−04	1.99
	1/32	5.6058e−03	2.07	6.8040e−04	2.00	1.5219e−04	2.00
	1/64	1.3029e−03	2.11	1.6959e−04	2.00	3.7443e−05	2.02

In Tables 1 and 2, we list the errors and convergence orders of our method on different meshes with $k = 1, 2$ and $c_0 = 0$, which are in agreement with theoretical predictions. Moreover, Figure 2 gives the error results for $c_0 = 0.5$ and shows the similar convergence trend.

Then, we also test a coupled CG-mixed virtual element method that uses the lowest-order continuous virtual element for the displacement and the lowest-order Raviart–Thomas-like virtual element for the flow variables [65]. In Table 3, it is clear to see the Poisson-locking effects (*i.e.*, the errors of the displacement stagnate on the coarser triangular and quadrilateral meshes) when the CG-mixed virtual element is used, while this phenomenon does not appear in Table 1 and the third column and $k = 2$ in Table 3. Therefore, we can conclude that our method is Poisson-locking-free even for a nearly incompressible material case.

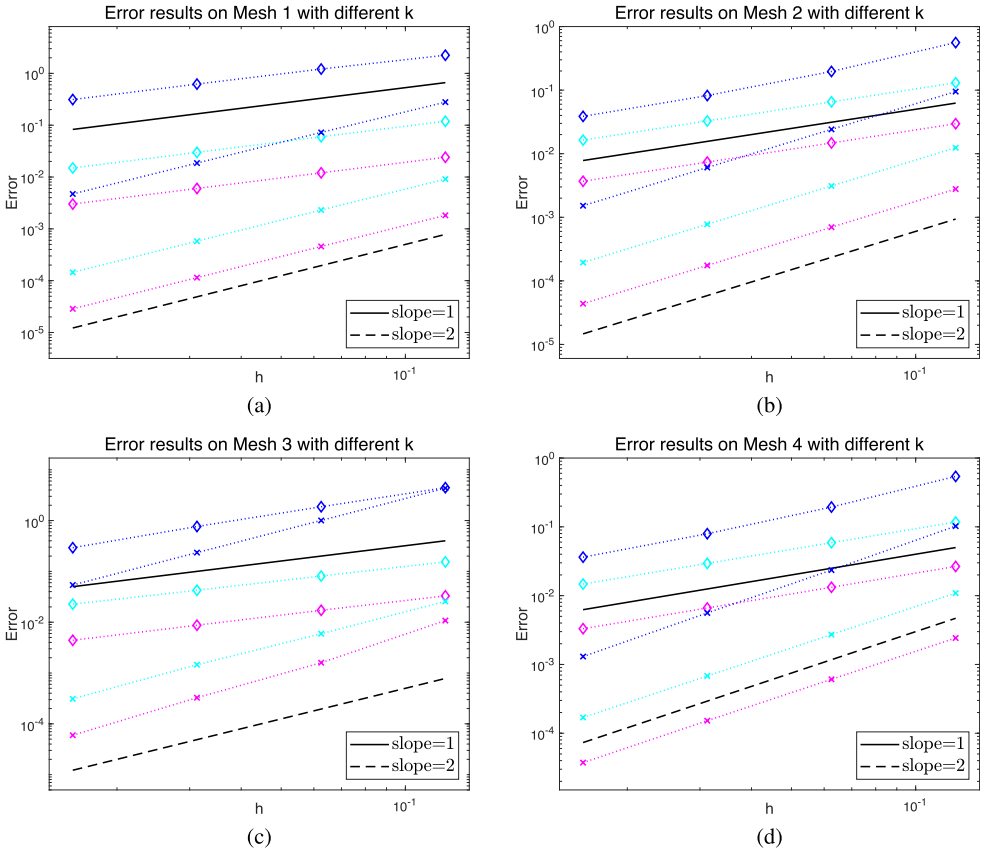

FIGURE 2. Convergence results on different meshes for $c_0 = 0.5$ (the blue, cyan and magenta lines respectively represent $\mathrm{err}_{\mathbf{u}}$, $\mathrm{err}_{\mathbf{q}}$, and err_p; the shapes $\diamond, \times$ respectively represent the numerical results for $k = 1, 2$). (a) $\mathcal{T}_h^1$. (b) $\mathcal{T}_h^2$. (c) $\mathcal{T}_h^3$. (d) $\mathcal{T}_h^4$.

TABLE 3. Displacement error results of CG-mixed virtual element method for $c_0 = 0$.

		$\mathcal{T}_h^1$		$\mathcal{T}_h^2$		$\mathcal{T}_h^3$	
k	h	$\mathrm{err}_{\mathbf{u}}$	Rate	$\mathrm{err}_{\mathbf{u}}$	Rate	$\mathrm{err}_{\mathbf{u}}$	Rate
1	1/8	3.1855e+00	–	3.2834e−01	–	6.0284e−01	–
	1/16	3.2479e+00	–	2.0961e−01	0.65	2.1880e−01	1.46
	1/32	3.2636e+00	–	1.3222e−01	0.66	6.6073e−02	1.73
	1/64	3.2675e+00	–	7.4493e−02	0.83	1.8051e−02	1.87
2	1/8	5.5291e−01	–	4.3524e−01	–	5.3273e−01	–
	1/16	1.4301e−01	1.95	8.7751e−02	2.31	1.3305e−01	2.00
	1/32	3.3945e−02	2.07	1.7408e−02	2.33	3.2905e−02	2.02
	1/64	8.2941e−03	2.03	3.6601e−03	2.25	8.2896e−03	1.99

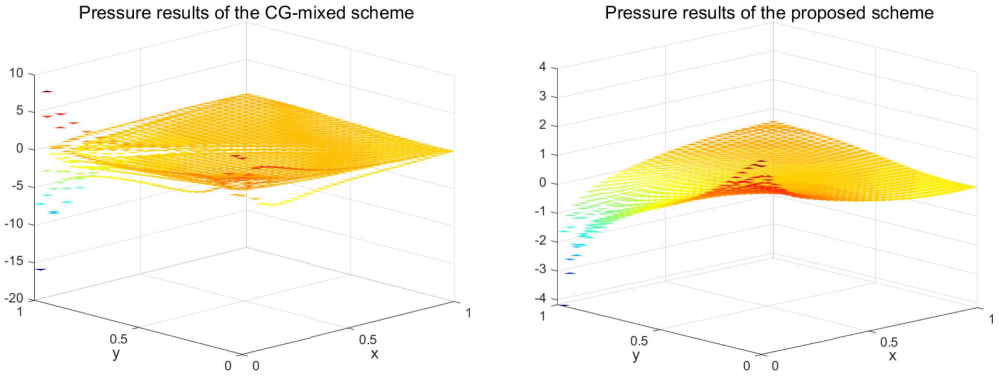

FIGURE 3. Pressure results of the cantilever bracket problem at time $t = 0.001$ using the CG-mixed method (*left*) and our method (*right*).

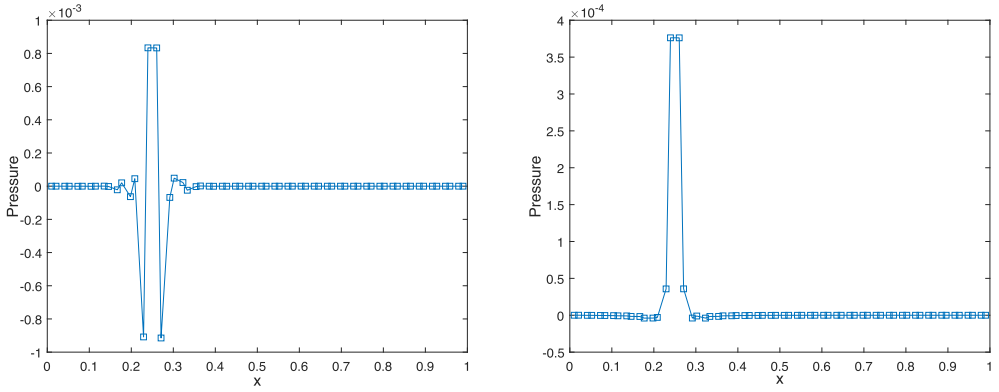

FIGURE 4. Pressure results of the Barry and Mercer's problem along the diagonal of the domain at time $t = 10^{-4}$ using the CG-mixed method (*left*) and our method (*right*).

4.2. Pressure-oscillation test

Here, in order to show the eliminated pressure oscillations, we need to consider the simulation results on a uniform triangulation of the unit square $\Omega := [0, 1]^2$ under parameters $k = 1, c_0 = 0$ and $\kappa \to 0$. Moreover, we set the body force $\mathbf{f}$, the initial displacement, and the initial pressure to be zero, and use Young's modulus E and Poisson's ratio ν to show Lamé constants:

$$\lambda = \frac{E\nu}{(1+\nu)(1-2\nu)}, \qquad \mu = \frac{E}{2(1+\nu)}.$$

For the cantilever bracket problem [25], we impose a no-flow boundary condition $\mathbf{q} \cdot \mathbf{n} = 0$ along all sides; the displacement on the left edge is fixed, *i.e.*, $\mathbf{u} = \mathbf{0}$; there is a downward traction at the top edge and a traction-free boundary condition at the right and bottom edges. Then, we set $\tau = 0.001, h = 1/32$ and use the material parameters $\alpha = 0.93, E = 10^4, \nu = 0.4, \kappa = 10^{-8}$.

Figure 3 shows a comparison of the numerical pressure results after one time step using the CG-mixed method and our method. It clearly shows that the CG-mixed method mainly produces spurious oscillations at the upper-left and lower-left corners, while the numerical pressure results obtained from our method do not suffer from these oscillations.

For the Barry and Mercer problem [66], we consider the time-independent boundary conditions:

$$\mathbf{u}\cdot\mathbf{t}_k = 0, \quad \mathbf{n}_k^T\nabla\mathbf{u}\mathbf{n}_k = 0, \quad p = 0,$$

and give a periodic pointwise source $g = \delta(\mathbf{x}-\mathbf{x}_0)\sin(\hat{t})$ with location $\mathbf{x}_0 = (1/4, 1/4)$ and the normalized time $\hat{t} = (\lambda+2\mu)\kappa t$. Then, we set $\tau = 10^{-4}, h = 1/32$ and use the material parameters $\alpha = 1, E = 10^5, \nu = 0.1, \kappa = 10^{-7}$.

Figure 4 shows a comparison of the numerical pressure results after one time step along the diagonal $(0,0) - (1,1)$ of the domain using the CG-mixed method and our method. One can observe the nonphysical pressure oscillations from the CG-mixed method, while nearly all oscillations have been eliminated by our method.

5. Conclusions

In this paper, our proposed method employs the Raviart–Thomas-like virtual element space for the flow variables and the divergence-free nonconforming virtual element for the displacement in Biot's consolidation model. We have presented a stability result for this fully discrete method that guarantees the existence and uniqueness of a solution at each time step and have derived an optimal convergence rate for the displacement in the $[\ell^\infty(0,T;H^1(\Omega))]^2$ norm, the pressure in the $\ell^\infty(0,T;L^2(\Omega))$ norm, and the fluid velocity in the $[\ell^2(0,T;L^2(\Omega))]^2$ norm. Finally, we have presented several numerical experiments that illustrate the convergence of the method with different meshes and different approximation accuracies, and the effectiveness in overcoming two modes of locking phenomena (*i.e.*, Poisson's locking and pressure oscillations) under a certain set of parameters.

Acknowledgements. The authors thank the support from the Youth Innovation Team (on computationally efficient numerical methods based on new energy problems) of Shaanxi Universities.

Funding. This research was supported in part by National Natural Science Foundation of China (No. 11901462, No. 12371405), Natural Science Foundation of Shaanxi Province (No. 2020JQ-130), and the fellowship of China Postdoctoral Science Foundation (No. 2020M683546).

References

[1] K. Terzaghi, Theoretical Soil Mechanics. Wiley, New York (1943).
[2] M.A. Biot, General theory of three-dimensional consolidation. *J. Appl. Phys.* **12** (1941) 155–164.
[3] M.A. Biot, Theory of elasticity and consolidation for a porous anisotropic solid. *J. Appl. Phys.* **26** (1955) 182–185.
[4] Y.K. Cheung and L.G. Tham, Numerical solutions for Biot's consolidation of layered soil. *J. Eng. Mech.* **109** (1983) 669–679.
[5] H.F. Wang, Theory of Linear Poroelasticity with Application to Geomechanics and Hydrogeology. Princeton University Press, Princeton (2000).
[6] J.P. Morris, W.W. McNab, S.K. Carroll, Y. Hao, W. Foxall and J.L. Wagoner, Injection and reservoir hazard management: the role of injection-induced mechanical deformation and geochemical alteration at in Salah CO_2 storage project. Gcags Transactions (2011).
[7] J.P. Morris, Y. Hao, W. Foxall and W.W. McNab, A study of injection-induced mechanical deformation at the in Salah CO_2 storage project. *Int. J. Greenhouse Gas Control* **5** (2011) 270–280.
[8] K. Strehlow, J.H. Gottsmann and A.C. Rust, Poroelastic responses of confined aquifers to subsurface strain and their use for volcano monitoring. *Solid Earth* **6** (2015) 1207–1229.
[9] C.C. Swan, R.S. Lakes and R.A. Brand, Micromechanically based poroelastic modeling of fluid flow in Haversian bone. *J. Biomech. Eng.* **125** (2003) 25–37.
[10] A.F.T. Mak, L.D. Huang and Q.Q. Wang, A biphasic poroelastic analysis of the flow dependent subcutaneous tissue pressure and compaction due to epidermal loadings-issues in pressure sore. *ASME. J. Biomech. Eng.* **116** (1994) 421–429.
[11] M. Yang and L.A. Taber, The possible role of poroelasticity in the apparent viscoelastic behavior of passive cardia muscle. *J. Biomech.* **24** (1991) 587–597.
[12] A. Halder, A. Dhall and A.K. Datta, Modeling transport in porous media with phase change: applications to food processing. *J. Heat Transfer* **133** (2010) 031010.
[13] S. Badia, A. Quaini and A. Quarteroni, Coupling Biot and Navier–Stokes equations for modelling fluid-poroelastic media interaction. *J. Comput. Phys.* **228** (2009) 7986–8014.
[14] K. Lipnikov, *Numerical methods for the Biot model in poroelasticity.* Ph.D. thesis, University of Houston (2002).
[15] R. Ewing, O. Iliev, R. Lazarov and A. Naumovich, On convergence of certain finite volume difference discretizations for 1D poroelasticity interface problems. *Numer. Methods Part. Differ. Equ.* **23** (2007) 652–671.

[16] F.J. Gaspar, F.J. Lisbona and P.N. Vabishchevich, Finite difference schemes for poroelastic problems. *Comput. Methods Appl. Math.* **2** (2002) 132–142.
[17] A. Naumovich, *Efficient numerical methods for the Biot poroelasticity system in multilayered domains*. Ph.D. thesis, University of Kaiserslautern (2007).
[18] A. Naumovich, On finite volume discretization of the three-dimensional Biot poroelasticity system in multilayer domains. *Comput. Meth. App. Math.* **6** (2006) 306–325.
[19] M.A. Murad and A.F.D. Loula, Improved accuracy in finite element analysis of Biot's consolidation problem. *Comput. Methods Appl. Mech. Eng.* **95** (1992) 359–382.
[20] M.A. Murad and A.F.D. Loula, On stability and convergence of finite element approximations of Biot's consolidation problem. *Int. J. Numer. Methods Eng.* **37** (1994) 645–667.
[21] M.A. Murad, V. Thomée and A.F.D. Loula, Asymptotic behavior of semidiscrete finite-element approximations of Biot's consolidation problem. *SIAM J. Numer. Anal.* **33** (1996) 1065–1083.
[22] R.W. Lewis and B.A. Schrefler, The Finite Element Method in the Static and Dynamic Deformation and Consolidation of Porous Media. Wiley, New York (1998).
[23] P.J. Phillips and M.F. Wheeler, A coupling of mixed and continuous Galerkin finite element methods for poroelasticity I: the continuous in time case. *Comput. Geosci.* **11** (2007) 131–144.
[24] P.J. Phillips and M.F. Wheeler, A coupling of mixed and continuous Galerkin finite element methods for poroelasticity II: the discrete-in-time case. *Comput. Geosci.* **11** (2007) 145–158.
[25] P.J. Phillips and M.F. Wheeler, Overcoming the problem of locking in linear elasticity and poroelasticity: an heuristic approach. *Comput. Geosci.* **13** (2009) 5–12.
[26] S.Y. Yi, A study of two modes of locking in poroelasticity. *SIAM J. Numer. Anal.* **55** (2017) 1915–1936.
[27] C. Rodrigo, F.J. Gaspar, X. Hu and L.T. Zikatanov, Stability and monotonicity for some discretizations of the Biot's consolidation model. *Comput. Methods Appl. Mech. Eng.* **298** (2016) 183–204.
[28] S.Y. Yi, A coupling of nonconforming and mixed finite element methods for Biot's consolidation model. *Numer. Methods Part. Differ. Equ.* **29** (2013) 1749–1777.
[29] X. Hu, C. Rodrigo, F.J. Gaspar and L.T. Zikatanov, A nonconforming finite element method for the Biot's consolidation model in poroelasticity. *J. Comput. Appl. Math.* **310** (2017) 143–154.
[30] B. Rivière, J. Tan and T. Thompson, Error analysis of primal discontinuous Galerkin methods for a mixed formulation of the Biot equations. *Comput. Math. Appl.* **73** (2017) 666–683.
[31] P.J. Phillips and M.F. Wheeler, A coupling of mixed and discontinuous Galerkin finite element methods for poroelasticity. *Comput. Geosci.* **12** (2008) 417–435.
[32] M. Sun and H.X. Rui, A coupling of weak Galerkin and mixed finite element methods for poroelasticity. *Comput. Math. Appl.* **73** (2017) 804–823.
[33] J. Wan, *Stabilized finite element methods for coupled geomechanics and multiphase flow*. Ph.D. thesis, Stanford University (2002).
[34] L. Berger, R. Bordas, D. Kay and S. Tavener, Stabilized lowest-order finite element approximation for linear three-field poroelasticity. *SIAM J. Sci. Comput.* **37** (2015) A2222–A2245.
[35] J.A. White and R.I. Borja, Stabilized low-order finite elements for coupled solid-deformation/fluid-diffusion and their application to fault zone transients. *Comput. Methods Appl. Mech. Eng.* **197** (2008) 4353–4366.
[36] D. Boffi, M. Botti and D.A. Di Pietro, A nonconforming high-order method for the Biot problem on general meshes. *SIAM J. Sci. Comput.* **38** (2016) A1508–A1537.
[37] R. Oyarzú and R. Ruiz-Baier, Locking-free finite element methods for poroelasticity. *SIAM J. Numer. Anal.* **54** (2016) 2951–2973.
[38] F.Z. Gao, A high-order HDG method for the Biot's consolidation model. *Comput. Math. Appl.* **77** (2019) 237–252.
[39] M.F. Wheeler, G. Xue and I. Yotov, Coupling multipoint flux mixed finite element methods with continuous Galerkin methods for poroelasticity. *Comput. Geosci.* **18** (2014) 57–75.
[40] J. Korsawe and G. Starke, A least-squares mixed finite element method for Biot's consolidation problem in porous media. *SIAM J. Numer. Anal.* **43** (2005) 318–339.
[41] L. Beirão da Veiga, F. Brezzi, A. Cangiani, G. Manzini, L.D. Marini and A. Russo, Basic principles of virtual element methods. *Math. Mod. Meth. Appl. Sci.* **23** (2013) 199–214.
[42] L. Beirão da Veiga, F. Brezzi, L.D. Marini and A. Russo, The hitchhiker's guide to the virtual element method. *Math. Mod. Meth. Appl. Sci.* **24** (2014) 1541–1573.
[43] L. Beirão da Veiga and G. Manzini, A virtual element method with arbitrary regularity. *IMA J. Numer. Anal.* **34** (2014) 759–781.
[44] B. Ayuso de Dios, K. Lipnikov and G. Manzini, The nonconforming virtual element method. *ESAIM: Math. Model. Numer. Anal.* **50** (2016) 879–904.
[45] L. Beirão da Veiga, F. Brezzi, L.D. Marini and A. Russo, H(div) and H(curl)-conforming virtual element methods. *Numer. Math.* **133** (2016) 303–332.
[46] F. Brezzi, R.S. Falk and L.D. Marini, Basic principles of mixed virtual element methods. *ESAIM: Math. Model. Numer. Anal.* **48** (2014) 1227–1240.
[47] L. Beirão da Veiga, F. Brezzi and L.D. Marini, Virtual elements for linear elasticity problems. *SIAM J. Numer. Anal.* **51** (2013) 794–812.

[48] A.L. Gain, C. Talischi and G.H. Paulino, On the virtual element method for three-dimensional elasticity problems on arbitrary polyhedral meshes. *Comput. Methods Appl. Mech. Eng.* **282** (2014) 132–160.
[49] E. Artioli, L. Beirão da Veiga, C. Lovadina and E. Sacco, Arbitrary order 2D virtual elements for polygonal meshes: part I, elastic problem. *Comput. Mech.* **60** (2017) 355–377.
[50] P.F. Antonietti, L. Beirão da Veiga, D. Mora and M. Verani, A stream virtual element formulation of the Stokes problem on polygonal meshes. *SIAM J. Numer. Anal.* **52** (2014) 386–404.
[51] X. Liu, R. Li and Y.F. Nie, A divergence-free reconstruction of the nonconforming virtual element method for the Stokes problem. *Comput. Methods Appl. Mech. Eng.* **372** (2020) 113351.
[52] F. Brezzi and L.D. Marini, Virtual element method for plate bending problems. *Comput. Methods Appl. Mech. Eng.* **253** (2012) 455–462.
[53] P.F. Antonietti, G. Manzini and M. Verani, The fully nonconforming virtual element method for biharmonic problems. *Math. Models Methods Appl. Sci.* **28** (2018) 387–407.
[54] M.F. Benedetto, S. Berrone, S. Pieraccini and S. Scialò, The virtual element method for discrete fracture network simulations. *Comput. Methods Appl. Mech. Eng.* **280** (2014) 135–156.
[55] S. Berrone, M.F. Benedetto, A. Borio, S. Pieraccini and S. Scialò, The virtual element method for large scale discrete fracture network simulations: fracture-independent mesh generation. *Proc. Appl. Math. Mech.* **15** (2015) 19–22.
[56] P.F. Antonietti, L. Beirão da Veiga, S. Scacchi and M. Verani, A C^1 virtual element method for the Cahn–Hilliard equation with polygonal meshes. *SIAM J. Numer. Anal.* **54** (2016) 34–56.
[57] X. Liu, Z.K. He and Z. Chen, A fully discrete virtual element scheme for the Cahn–Hilliard equation in mixed form. *Comput. Phys. Commun.* **246** (2020) 106870.
[58] J.K. Zhao, B. Zhang, S.P. Mao and S.C. Chen, The divergence-free nonconforming virtual element for the Stokes problem. *SIAM J. Numer. Anal.* **57** (2019) 2730–2759.
[59] X.L. Tang, Z.B. Liu, B.J. Zhang and M.F. Feng, On the locking-free three-field virtual element methods for Biot's consolidation model in poroelasticity. *ESAIM: Math. Model. Numer. Anal.* **55** (2021) S909–S939.
[60] L. Beirão da Veiga, F. Brezzi, L.D. Marini and A. Russo, Virtual element methods for general second order elliptic problems on polygonal meshes. *Math. Mod. Meth. Appl. Sci.* **26** (2016) 729–750.
[61] L. Beirão da Veiga, L. Mascotto and J. Meng, Interpolation and stability estimates for edge and face virtual elements of general order. *Math. Models Methods Appl. Sci.* **32** (2022) 1589–1632.
[62] J.K. Zhao, B. Zhang, S.P. Mao and S.C. Chen, The nonconforming virtual element method for the Darcy–Stokes problem. *Comput. Methods Appl. Mech. Eng.* **370** (2020) 113251.
[63] K. Mardal and R. Winther, An observation on Korn's inequality for nonconforming finite element methods. *Math. Comput.* **75** (2005) 1–6.
[64] S.C. Brenner, Korn's inequalities for piecewise H^1 vector fields. *Math. Comput.* **73** (2004) 1067–1087.
[65] X. Liu and Z. Chen, Coupling of mixed and conforming virtual element approximations for three-field poroelasticity, submitted.
[66] S. Barry and G. Mercer, Exact solution for two-dimensional time dependent flow and deformation within a poroelastic medium. *J. Appl. Mech.* **66** (1999) 536–540.